the plant journal

SEB SOCIETY FOR EXPERIMENTAL BIOLOGY

The Plant Journal (2025) **124,** e70613 doi: 10.1111/tpj.70613

Regulation of tomato fruit growth and development during different plant developmental stages by far-red light: a combined anatomical, physiological, and transcriptomic analysis

Maria Mastoraki[1], Sofia Bengoa Luoni[2], Julia Lindeboom[1], Ep Heuvelink[1,*] and Leo F.M. Marcelis[1]

[1]*Horticulture and Product Physiology, Department of Plant Sciences, Wageningen University & Research, Wageningen, The Netherlands, and*

[2]*Laboratory of Genetics, Wageningen University and Research, Wageningen, The Netherlands*

Received 2 July 2025; revised 15 October 2025; accepted 17 November 2025.

*For correspondence (e-mail ep.heuvelink@wur.nl)

SUMMARY

Far-red (FR) light, a critical environmental signal perceived via phytochrome photoreceptors, modulates numerous aspects of plant development; yet, its role in reproductive processes such as fruit growth and ripening remains less clear. In this study, we investigated the developmental stage-specific effects of FR light on fruit development, anatomy, and metabolism in dwarf tomato (*Solanum lycopersicum*) plants. FR light was applied during three distinct stages: vegetative phase, early fruit development, and late fruit development. Three corresponding plant batches were analyzed: (i) full-growth cycle plants for final fruit weight and plant architecture, (ii) plants harvested at the mature green stage for anatomical measurements, and (iii) plants during early fruit formation for integrated transcriptomic and metabolomic profiling of source (leaf) and sink (fruit) tissues. FR exposure from flowering to the full-grown green fruit stage increased total fruit weight by enhancing fruit size, linked to an increase in both mesocarp cell layers and cell size. These anatomical changes were associated with transcriptional upregulation of genes related to auxin, gibberellins, and brassinosteroid biosynthesis and signaling in both leaves and fruits. Additionally, FR light accelerated the onset of ripening, coinciding with transcriptional upregulation of abscisic acid and ethylene biosynthesis pathways. Furthermore, our results reveal that FR light is initially perceived in leaves and subsequently modulates fruit development and ripening through hormone-mediated signaling. This study provides new insights into the light-regulated plasticity of reproductive development and highlights the importance of FR timing in optimizing fruit fresh weight and sugar content.

Keywords: cells, far-red, fruit growth, hormones, ripening, *Solanum lycopersicum*, tomato fruit.

INTRODUCTION

Light is a central environmental signal that profoundly influences plant development, physiology, and metabolic processes. In addition to its role as an energy source, light spectrum—specifically the ratio of red (R 600–700 nm) to far-red (FR 700–800 nm) wavelengths—serves as a key indicator of competition and neighbor plant proximity in natural and agricultural environments (Roig-Villanova & Martínez-García, 2016; Ballaré & Pierik, 2017; Huber et al., 2021; Casal & Fankhauser, 2023; Huber et al., 2024). Plants perceive changes in the red: far-red (R:FR) light ratio through the phytochrome photoreceptor, which is reversibly interconverted by light between its inactive form, Pr, and its physiologically active form, Pfr, with peaks in absorption in the red and far-red regions of the spectrum, respectively (Borthwick et al., 1952; Sager et al., 1988). A reduction in R:FR ratio, typical of vegetative shading or dense plantings, triggers a cascade of reactions that lead to morphological and physiological changes collectively known as the shade avoidance syndrome (SAR), including rapid elongation of stems and leaves, and altered allocation of resources (Ballaré & Pierik, 2017; Casal, 2013; Franklin, 2008).

Most of our knowledge on mechanisms orchestrating shade avoidance comes from studies on *Arabidopsis thaliana*. Briefly, it is well documented that FR detection in leaves inactivates phytochrome B, which in turn leads to the accumulation of active phytochrome interacting factor (PIF) transcription factors. PIFs stimulate the auxin synthesis

pathway, and auxin is then translocated to the different organs to trigger cell expansion, which leads to organ elongation (Pierik & Ballaré, 2021). In tomato (*Solanum lycopersicum*), a widely cultivated crop and model plant with strong photomorphogenic sensitivity, responses to FR have been studied in the context of vegetative growth and architecture (Demotes-Mainard et al., 2016). FR radiation has been shown to induce internode elongation, increase leaf expansion, affect biomass partitioning, and enhance apical dominance (Ji et al., 2021; Kalaitzoglou et al., 2019; Li et al., 2015; Shomali et al., 2024; Song et al., 2024). While several studies, including those by Kalaitzoglou et al. (2019) and Ji et al. (2020) have reported that FR light can influence carbon allocation and favor resource partitioning toward fruits, a comprehensive understanding of how FR modulates reproductive traits, such as fruit development, composition, and quality is missing. Given the commercial and nutritional importance of tomato fruit, understanding how FR light influences fruit-associated traits is of both fundamental and applied interest.

Moreover, while previous work has identified physiological and hormonal pathways responsive to FR light, the developmental stage at which FR may critically influence the direction and magnitude of these responses remains unknown. In this study, we aim to investigate: (1) the effects of far-red light exposure at different plant developmental stages on morphological traits, fruit anatomy, and growth in tomato, and (2) the associated changes in early metabolism and gene expression in both vegetative and reproductive organs. To address these knowledge gaps, we implemented an integrative, multilevel approach combining morphological and physiological assessments with transcriptomic (RNA-sequence) and untargeted metabolomic profiling of leaves and fruits. We hypothesized that the developmental period spanning from flowering to the full-grown green fruit stage represents the critical window during which FR exerts the greatest influence on fruit anatomical development, carbohydrate content, and final fruit fresh weight. Specifically, we hypothesize that FR exposure during this stage significantly alters pericarp cell histology, through modulation of endogenous hormone levels.

RESULTS

Effects of timing of FR application on yield and whole plant morphology at the end of the growth cycle

The FR response is well known as an internal plant reaction to shading. Our results agree with this pattern: when FR was applied throughout the entire growth period, plants showed a larger fraction of biomass allocated to the stem compared with plants grown without FR, although this difference was not statistically significant (Figure 1a). Interestingly, the biomass fraction partitioned to the stem was significantly higher when FR was applied throughout the entire growth period, compared with FR applied from flowering until full-grown green fruits and FR applied from green fruits until red fruits.

When FR was applied during stages where fruits were present, the total plant dry mass remained unchanged compared with NO FR, but the dry mass partition to fruits was significantly increased, especially in the case of FR added from flowering until full-grown green fruits (Figure 1d,e). Furthermore, there was a tendency that FR applied throughout the entire growth period resulted in the highest fruit fresh weight, followed by FR from flowering until full-grown green fruits and FR from vegetative until flowering, although the difference was not statistically significant (Figure 1f).

Collectively, these results indicate that FR applied from flowering until full-grown green fruits excelled in fruit-focused dry biomass allocation, while FR applied throughout the entire growth period resulted in greater dry biomass allocation to the stem at the expense of leaves and did not affect the fruits.

Differential effects of timing of FR application on tomato fruit volume, number of trusses, and fruit number

Differences in fruit volume became evident after 16 DAA, with FR applied throughout the entire growth period resulting in the highest fruit volume (Figure 2b). From this stage onward, differences became more pronounced, with FR from flowering until full-grown green fruit stage reaching a volume statistically not different from FR applied throughout the entire growth period. By 43 DAA, both FR from flowering until full-grown green fruits and FR throughout the entire growth period attained peak fruit volume, while FR before flowering and FR from full-grown green fruits until ripe had the smallest fruits and did not differ from each other. As opposed to fruit volume, the number of trusses and the number of fruits per plant were not significantly affected by the FR treatments (Figure 2a,c).

Timing of FR application affects fruit color development and ripening

The effect of FR on skin color, expressed as the a^* value, was evaluated over time. This parameter, which reflects color variations along the red–green axis, served as an indicator of fruit ripening, with higher values signifying increased redness and maturation.

At 40 DAA, fruits from all treatments were still in the green fruit stage (Figure 2e). At 45 DAA, a^* values increased sharply when FR was applied throughout the entire growth period, indicating the transition to red fruits, while fruits in the other treatments were still green. By 47 DAA, the differences became more pronounced. Fruits from plants that received FR throughout the entire growth period maintained the highest a^* values. Fruits from plants that received FR from flowering until fully grown green fruits also began to show increases in a^*, distinguishing

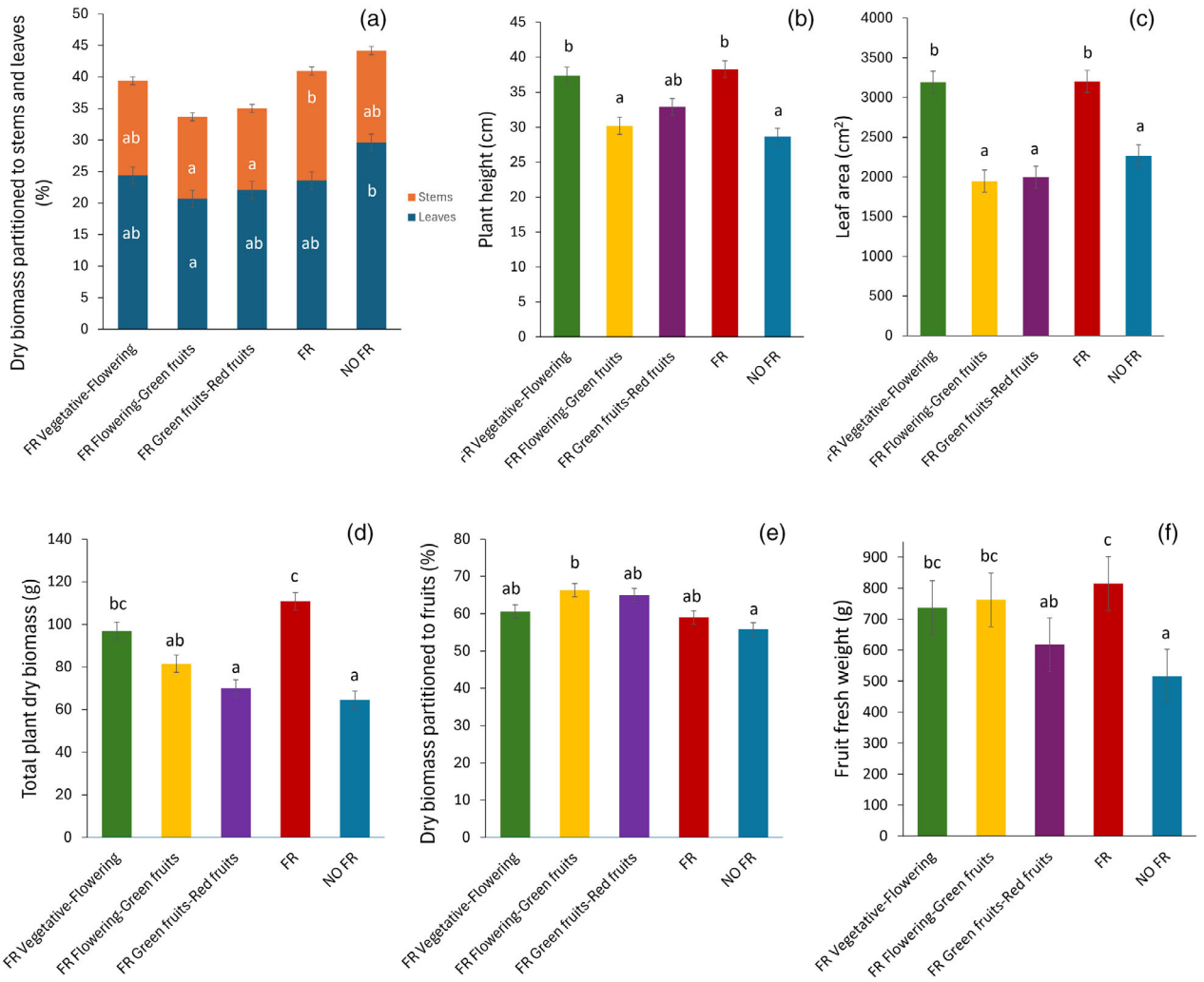

Figure 1. Effect of adding far-red (FR) at different plant developmental stages on tomato (*Solanum lycopersicum*) growth traits at the end of the growth cycle, 74 days after anthesis (DAA).
Shown are the fraction of dry biomass allocated to leaves and stems (a), final plant height (b), total leaf area (c), the total plant dry biomass (d), the fraction of dry biomass allocated to fruits (e), and total fruit fresh weight (f). Data represent means ± standard error ($n = 6$). Different letters indicate statistically significant differences between treatments according to Tukey's HSD test ($\alpha = 0.05$).

them from the other treatments. Additionally, the treatment with FR applied from vegetative to flowering stages showed higher *a** values compared with NO FR. At 50 DAA, fruits from plants exposed to FR throughout the entire growth period reached maturity and were harvested. Their *a** values did not differ statistically from those of fruits exposed to FR only from flowering until the full-grown green stage. Similarly, fruits from the FR vegetative–flowering treatment showed no significant differences compared with either of these groups, although their *a** values were slightly lower. By 53 DAA, fruits from FR from flowering until full-grown green fruits reached their peak *a** value and were harvested. Ripening of fruits from the other three treatments progressed more slowly, reaching maturation at 57 DAA.

Differential effects of timing of FR application on soluble sugar content in ripe tomato fruits

Red ripe fruits from plants where FR was applied throughout the entire growth cycle showed the highest total soluble sugar content, significantly exceeding all other treatments; however, not differing statistically from fruits of plants that received FR from flowering until full-grown green fruits. The other treatments did not differ from each other (Figure 2d).

Fruits from plants that received FR throughout the entire growth cycle and FR from flowering until full-grown green fruits had the highest glucose content, with no significant difference between them. The other three treatments showed the lowest glucose content and did not

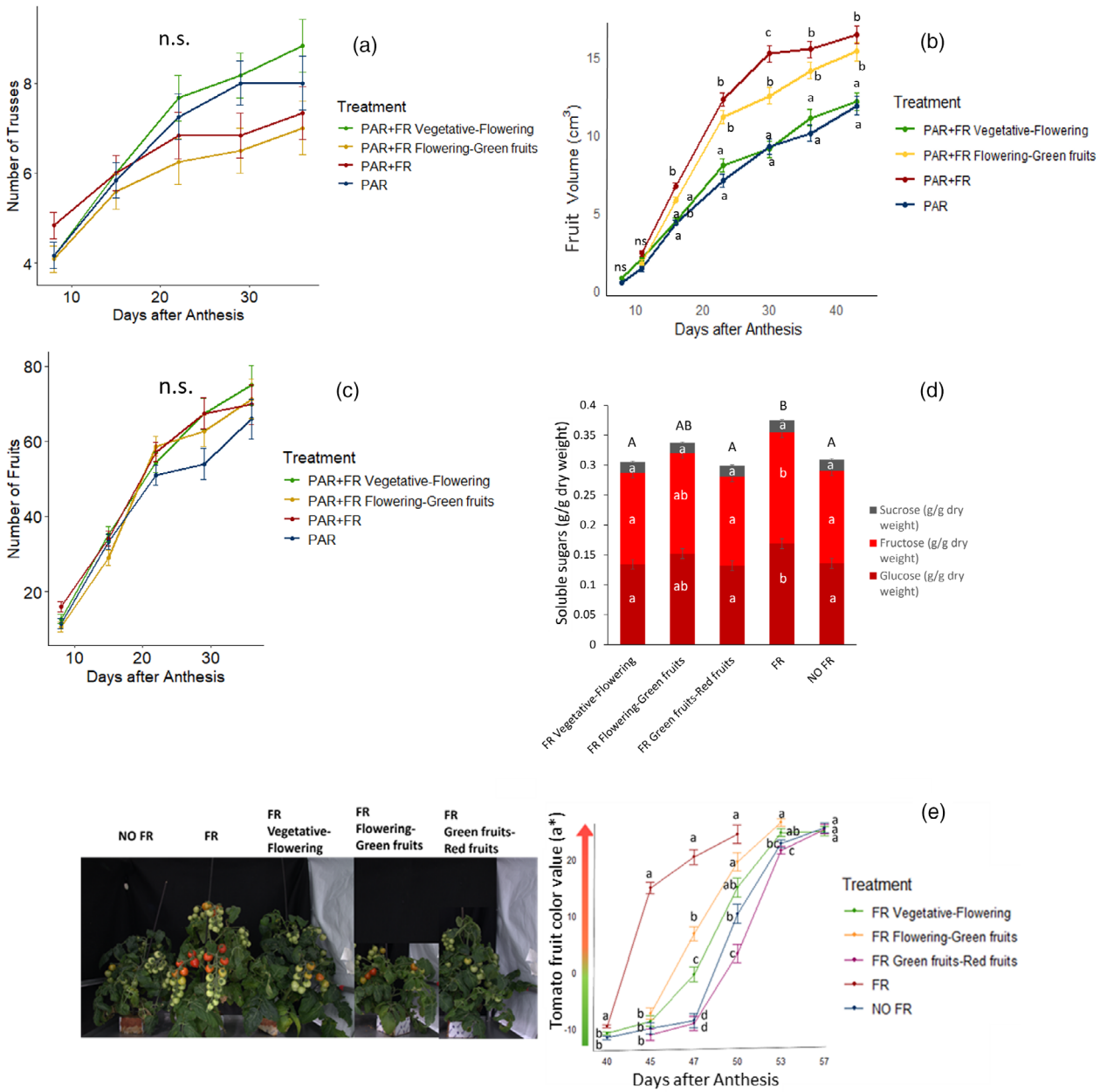

Figure 2. Effect of adding far-red (FR) at different plant developmental stages on tomato (*Solanum lycopersicum*) growth traits over time. Shown are: (a) number of trusses (measured from 8 to 36 days after anthesis [DAA]), (b) fruit volume (measured from 8 to 43 DAA), (c) number of fruits (measured from 8 to 36 DAA), (d) soluble sugar content in ripe fruits, and (e) fruit color change, measured from 40 to 57 DAA using the *a** value of the CIELAB color space, where higher *a** values indicate a shift toward red. In graphs (a), (b), and (c), the treatment FR Green fruits–Red fruits (starting at 38 DAA) is not shown, as it had not yet been initiated during the measurement periods. Data represent means ± standard error ($n = 6$). Different letters indicate statistically significant differences between treatments according to Tukey's HSD test ($\alpha = 0.05$).

differ from each other. Interestingly, the fructose content of fruits from plants that received FR throughout the entire growth cycle was significantly higher than that of all other treatments, followed by the treatment FR from flowering until full-grown green fruits. The other treatments did not differ from each other and had the lowest values. No significant difference was detected in fruit sucrose content between the FR treatments (Figure 2d).

Differential effects of timing of FR application on fruit carbohydrate content and anatomy

Collectively, the period from flowering until the full-grown green fruit stage is a critical window for FR application, regarding fruit growth, ripening, and sugar accumulation. To investigate the mechanisms behind this sensitivity, we analyzed fruit physiology at 35 DAA and conducted

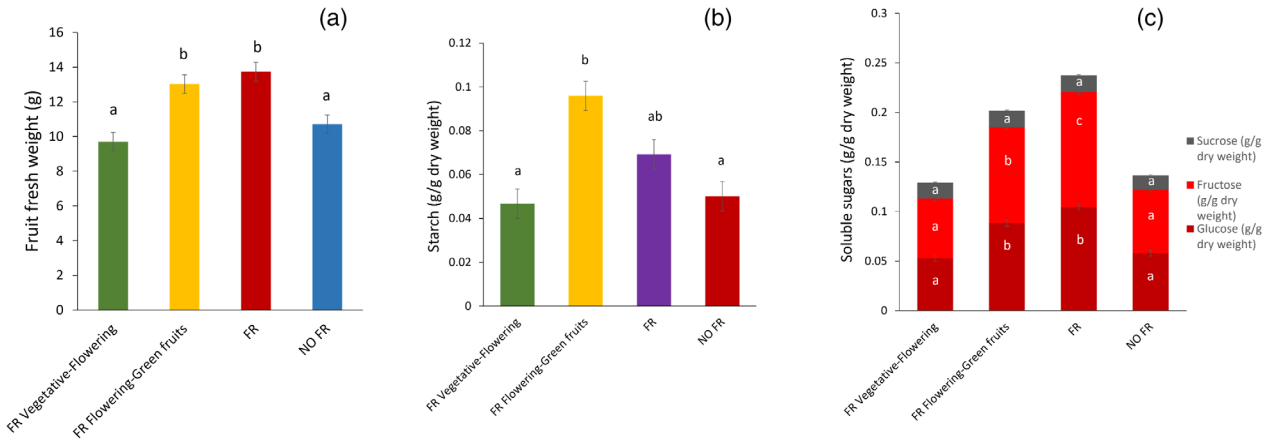

Figure 3. Effect of far-red (FR) light applied at different developmental stages up to 35DAA.
Shown are mean fruit fresh weight (a), starch (b), and soluble sugars content (c) in tomato (*Solanum lycopersicum*) fruits. The FR Green fruits–Red fruits treatment (initiated at 38 DAA) is not included, as the analysis was conducted at 35 DAA. Data represent means ± standard error ($n = 6$). Different letters indicate statistically significant differences between treatments according to Tukey's HSD test ($\alpha = 0.05$).

transcriptomic and metabolomic profiling of leaves and fruits at 10 DAA.

At 35 DAA, FR throughout the entire growth period and FR from flowering until full-grown green fruits resulted in the highest fruit fresh weights. Fruits from plants that received FR only before anthesis and NO FR did not differ from each other and showed the lowest fresh weights (Figure 3a).

Fruits receiving FR from flowering until full-grown-green fruits stage showed the highest starch content, although not significantly different from fruits on plants that received FR throughout the entire growth period. Fruits from plants that received NO FR and FR only before anthesis did not differ in starch content (Figure 3b).

Glucose content was significantly higher in fruits treated with FR throughout the entire growth period and FR from flowering until full-grown green fruits, compared with the other two treatments that did not differ from each other (Figure 3c). Fructose content was highest in FR throughout the entire growth period followed by the treatment FR from flowering until full-grown green fruits. No significant differences in sucrose content were observed between the FR treatments (Figure 3c).

To further investigate the cause underlying differences in fruit volume induced by FR, we analyzed its effects on pericarp cell histology. Fruits from plants receiving FR from flowering until the full-grown green fruit stage and fruits from plants receiving FR throughout the entire growth cycle showed the highest mesocarp volume, with no statistically significant differences between them (Figure 4a,b). However, the reason for the fruit volume increase was different between the two treatments. In treatment FR from flowering until green fruits, the increase in mesocarp volume was primarily attributed to a significant enlargement of mesocarp cell volume, accompanied by a moderate increase in the number of mesocarp cell layers (Figure 4c,d). Conversely, in treatment FR applied throughout the entire growth cycle, the increase in mesocarp volume was mainly driven by the highest number of mesocarp cell layers among all treatments, while mesocarp cell volume also increased but to a lesser extent, without a statistically significant difference compared with the FR flowering-to-green fruits treatment (Figure 4c,d).

In contrast, the treatment of FR from vegetative until flowering led to a significant increase in the number of mesocarp cell layers, similar to treatment FR from flowering until green fruits, resulting in the highest number of cell layers among treatments (Figure 4c). However, mesocarp cell volume remained unchanged, leading to a total mesocarp volume comparable to that observed in NO FR (Figure 4d).

To summarize the overall treatment effects on tomato plant morphology and carbohydrate traits, a hierarchical cluster analysis was performed using standardized values of selected traits. The clustered heatmap revealed differences among treatments based on both vegetative and reproductive parameters (Figure 5). FR from flowering until full-grown green fruits and FR throughout the entire growth cycle clustered closely together, indicating a similar effect on key fruit-associated parameters such as starch and sugar content, fruit volume, color transition, dry mass allocation to fruits, and fresh weight. However, these two treatments differed markedly in their influence on vegetative traits, including dry mass allocation to leaves and stems, plant height, and leaf area, suggesting a divergence

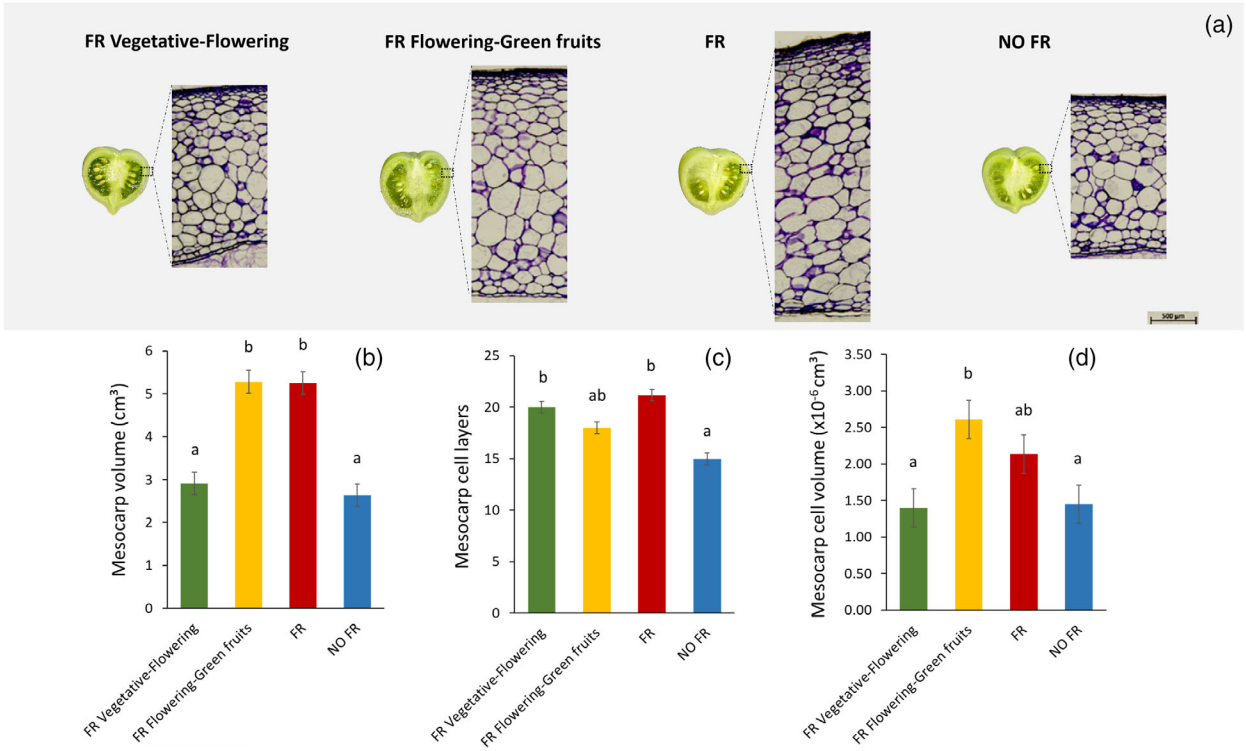

Figure 4. Image analysis of tomato (*Solanum lycopersicum*) fruit pericarp tissue sections as they were affected by far-red (FR) light applied at different plant developmental stages.
This figure displays microscopy images of pericarp sections (a), measurements on mesocarp volume (b), mesocarp cell layers (c), and mesocarp cell volume (d). Data represent means ± standard error ($n = 6$). Different letters indicate statistically significant differences between treatments according to Tukey's HSD test ($\alpha = 0.05$).

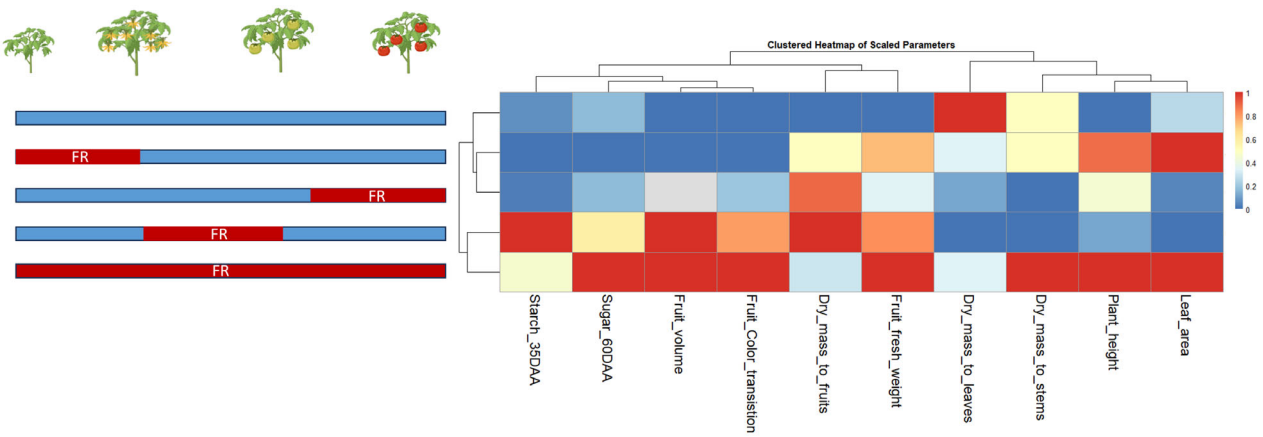

Figure 5. Hierarchical cluster analysis illustrating the overall effect of far-red (FR) light supplementation at different developmental stages on key physiological and anatomical traits in tomato (*Solanum lycopersicum*) plants.
The left side represents the treatments based on the developmental stage during which additional FR was applied. The heatmap on the right displays the relative effect of each treatment on the measured traits. Color intensity indicates the magnitude and direction of the effect, with red denoting a strong positive association and blue indicating a negative association between FR treatment and the corresponding trait.

in how carbon is partitioned between reproductive and vegetative sinks. In contrast, the other three treatments formed a distinct cluster characterized by a tendency to favor vegetative growth more strongly than reproductive development.

Transcriptomics on leaves and fruits

Leaves

FR affected total fruit fresh weight as well as different physiological parameters in the treatment FR from

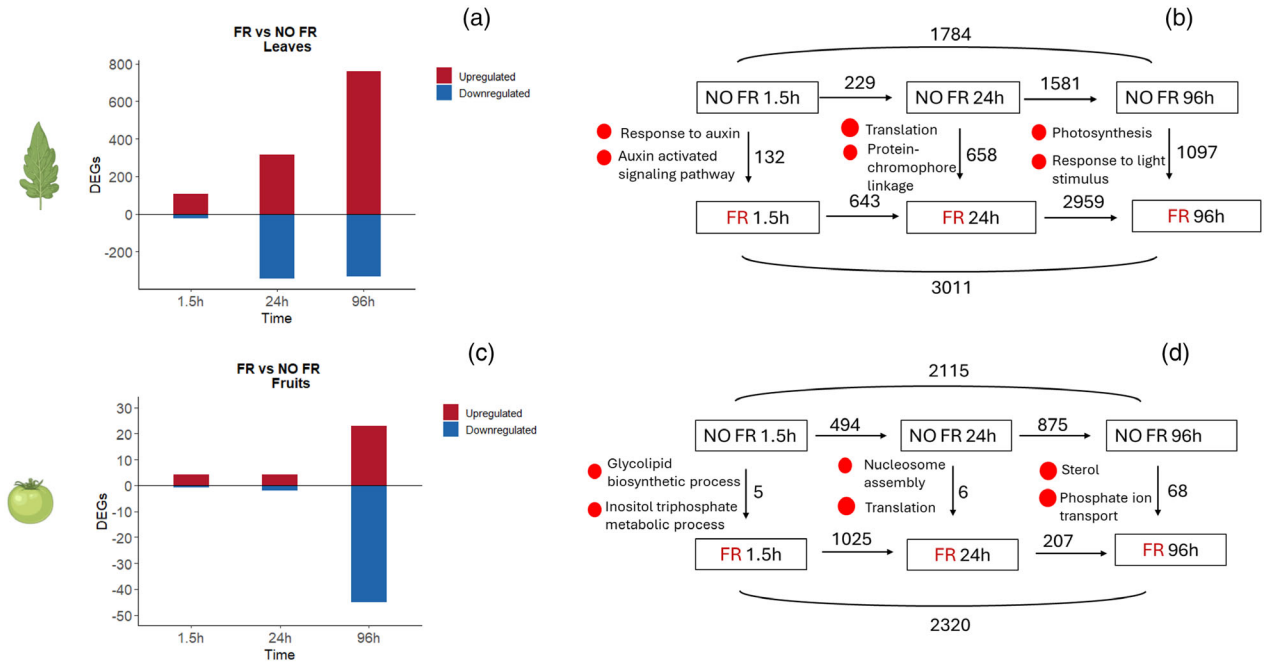

Figure 6. Transcriptomic responses to far-red (FR) light exposure in leaves and fruits over time.
(a) Number of differentially expressed genes (DEGs) in leaves exposed to FR compared with NO FR at 1.5, 24, and 96 h at 10 DAA. Red bars represent upregulated genes, and blue bars represent downregulated genes.
(b) DEG comparisons between time points in leaves under FR and NO FR conditions. Numbers on arrows indicate the number of DEGs between respective time points. Functional enrichment highlights auxin response at 1.5 h, translation and protein–chromophore linkage at 24 h, and photosynthesis and response to light stimulus at 96 h under FR conditions.
(c) Number of DEGs in fruits exposed to FR compared with NO FR at 1.5, 24, and 96 h after 10 DAA. Red bars represent upregulated genes, and blue bars represent downregulated genes.
(d) DEG comparisons between time points in fruits under FR and NO FR conditions. Numbers on arrows indicate the number of DEGs between respective time points. Functional enrichment highlights glycolipid biosynthesis and inositol triphosphate metabolism at 1.5 h, translation and nucleosome assembly at 24 h, and sterol and phosphate ion transport at 96 h under FR conditions.

flowering until full-grown green fruits. To investigate the regulatory gene pathways affected by the treatment, a transcriptomic analysis was conducted at 10 DAA.

Figure 6a,b illustrates the transcriptional response in leaves under FR compared with the absence of FR, across three time points: 1.5 , 24 , and 96 h (4 days) after exposure to FR. At 1.5 h, the number of differentially expressed genes (DEGs) was relatively low, but it increased significantly at 24 h and peaked at 96 h, particularly in the number of upregulated genes. Figure 6b summarizes the functional transitions over time. At 1.5 h under FR treatment, genes related to auxin response and auxin-activated signaling were enriched. At 24 h, enriched functions included translation and protein–chromophore linkage. By 96 h, the transcriptomic response was dominated by genes associated with photosynthesis and response to light stimuli.

Figure 6b also shows the DEGs across sampling times. In each time point comparison, the total number of DEGs under FR treatment is at least double the number observed in the absence of FR.

Gene grouping strategy—Genes were categorized into three groups—Green, Orange, and Purple—based on their expression patterns over time under the FR and NO FR conditions (Figure S4). Initially, we filtered genes for which the NO FR condition remained stable across all time points, to avoid genes whose expression is influenced by natural time-dependent processes. From this subset, we retained only those genes that showed a statistically significant difference (P-value <0.05) and an absolute log fold change (|logFC|) greater than 1 when comparing FR versus NO FR conditions.

The selected genes were then classified according to the time points at which differential expression was observed between FR and NO FR: Green group, genes that were significantly different between FR and NO FR at all three time points; Orange group, genes that were significantly different only at the first time point (1.5 h); Purple group, genes that were significantly different only at the last time point (96 h). A graphical representation of gene expression profiles is presented in Figure S4. Individual expression plots for each gene are available in Figures S5–

S7. A complete list of genes in each group can be found in the Supplementary RNA sequencing folder.

Description of genes in green group—The Green group comprised 37 genes, with 31 upregulated and 6 downregulated compared with the NO FR condition (Figure S5, Supplementary log2FC). Several of the upregulated genes are associated with auxin signaling (supporting the GO enrichment analysis presented in Figure 6b), including *Solyc08g068490.3* (auxin response factor 5), *Solyc01g110730.4* (auxin-responsive SAUR family protein), *Solyc01g110770.2* (auxin-induced protein), *Solyc08g062180.3* (auxin-responsive protein IAA29), *Solyc01g110790.3* (auxin-induced protein), *Solyc12g009240.2* (auxin-responsive GH3 family protein), and *Solyc03g118810.4* (auxin efflux carrier component). These genes are annotated with GO terms or Pfam domains linked to auxin responsiveness or signaling and consistently exhibit positive log fold changes across time points, indicating sustained upregulation.

In addition to auxin-related genes, others within this group are involved in broader hormonal signaling pathways, *Solyc01g080880.4* (*BRI1-associated receptor kinase*) and *Solyc07g062260.3* (brassinosteroid insensitive 1-like protein) are involved in brassinosteroid signaling, while *Solyc06g035530.3*, encoding gibberellin 20-oxidase, plays a role in gibberellin biosynthesis. These hormone-associated genes also show strong upregulation, suggesting that hormonal modulation is an integral component of the transcriptional response under the experimental conditions.

In terms of transcriptional regulation, many genes in the dataset are annotated with transcription factor activity, particularly those containing homeodomain or helix–loop–helix (HLH) motifs. These include *Solyc04g074700.4* (homeobox-leucine zipper protein HAT22), *Solyc02g091930.3* (basic helix–loop–helix transcription factor bHLH137), *Solyc08g078300.4* (basic helix–loop–helix protein bHLH92), *Solyc03g114720.3* (homeobox transcription factor KNAT3-like), *Solyc01g110770.2*, *Solyc01g110730.4*, and *Solyc01g110790.3* (all three annotated as auxin-induced transcription factors, likely from the SAUR family), as well as *Solyc07g062260.3* (brassinosteroid insensitive 1-like transcription factor) and *Solyc10g008270.3* (zinc finger homeodomain protein 1-like). All of these genes are upregulated, with log fold changes consistently above 1 across time points, suggesting a robust activation of transcription factor-mediated gene regulation. In contrast, *Solyc10g008270.3* shows downregulation, which may reflect repression of specific transcriptional programs in response to the treatment.

One gene stands out for its strong upregulation and functional relevance. *Solyc09g082620.3*, annotated with guard cell differentiation, shows consistent induction, suggesting enhanced cell differentiation processes. Additionally, three genes of unknown function—*Solyc10g084600.2*, *Solyc05g054750.3*, and *Solyc04g051470.1*—*are* also highly upregulated, indicating possible roles in uncharacterized but significant pathways.

Description of genes in Orange group

Transcription factors (TFs) are well-established as key regulators of gene expression networks. These genes often respond rapidly to environmental or developmental signals, initiating cascades that activate or repress downstream targets, ultimately influencing phenotype. Typically, after this initial activation, TFs are downregulated through negative feedback mechanisms. To investigate genes involved in the early response to FR, we focused on those that were significantly up- or downregulated (log FC >1, $p < 0.05$) exclusively at 1.5 h after FR exposure (Figure S4b). A total of 23 genes were differentially expressed specifically at 1.5 h. Among these nine genes were downregulated (Figure S6).

A notable number of genes encode TFs or are annotated with gene ontology (GO) terms related to transcriptional regulation. *Solyc01g100660.4* (*HSFA2*) and *Solyc06g069370.4* (*NAC083*), both nucleus-localized and involved in regulation of transcription (GO:0006355), were upregulated. Three TFs, *Solyc01g109700.3* (*bZIP61*), *Solyc07g062710.4* (*bHLH92*), and *Solyc08g080150.1* (*TCP20*), which contain bZIP, Helix–Loop–Helix, and TCP domains respectively, were also upregulated as well as the previously mentioned *Solyc04g053000.1* (ARF5), which displayed the highest upregulation across the dataset.

Several of the DEGs in this group are closely linked to hormone biosynthesis. *Solyc12g088300.2* (*IPT5*), annotated as being involved in cytokinin biosynthesis (GO:0009691), was strongly downregulated at 1.5 h (log2FC: −2.35). In contrast, *Solyc01g110710.3* (*IAA14*), an auxin-responsive gene, was clearly upregulated at 1.5 h and 96 h, supporting the activation of auxin signaling during early and later phases. *Solyc04g053000.1* (*ARF5*), also auxin-related and involved in transcription regulation, showed very strong upregulation at all time points (log2FC: 4.69 at 1.5 h), highlighting a robust auxin-mediated transcriptional reprogramming. Another auxin-related gene, *Solyc07g006310.1* (*GH3.9*), showed similar trends. Additionally, *Solyc06g008870.2* (*GID1B*), associated with gibberellic acid-mediated signaling (GO:0009740) and floral development, showed upregulation, indicating a potential role in hormone crosstalk and developmental processes.

Description of genes in purple group—A total of 185 genes were identified in the purple group, of which 155 were upregulated and 30 were downregulated (Figure S4c, Supplementary log2FC, Figure S7).

The dataset shows a strong emphasis on transcriptional control, particularly through GO terms such as GO:0006355 (regulation of transcription, DNA-templated)

and GO:0006357 (regulation of transcription by RNA polymerase II). These processes are essential for fine-tuning gene expression in response to both internal developmental cues and external environmental signals. The presence of multiple regulators, including those involved in chromatin dynamics like histone exchange (GO:0043486) and chromatin assembly regulation (GO:0010847), suggests active remodeling of the transcriptional landscape. This likely supports a flexible gene expression program needed during growth, differentiation, or stress adaptation.

A total of 18 genes were annotated as TFs, with all but one (*Solyc04g077220.3*) showing upregulation. Several genes, including *Solyc01g095100.4*, *Solyc01g095630.3*, *Solyc04g078550.3*, *Solyc06g068460.3*, and *Solyc10g011910.4*, encode WRKY domain TFs, which are implicated in leaf development and stress responses. Key transcription factor families such as MADS-box proteins (e.g., *Solyc04g081000.3*, *Solyc05g015750.3*, *Solyc06g059970.4*) play crucial roles in regulating floral organ identity and developmental processes. Additionally, members of the GRAS (*Solyc02g085600.1*) and SBP (*Solyc02g077920.4*) families highlight regulation of growth, hormone signaling , and flower development. The presence of diverse TF domains including bHLH, TCP, bZIP, and homeobox further reflects complex transcriptional networks integrating environmental cues, circadian rhythms, and developmental sig nals to finely tune gene expression in tomato.

Several genes related to plant hormone signal transduction show differential expression. For instance, *Solyc05g056440.3* (fold change −1.10) is downregulated and encodes a Small Auxin-Up RNA (SAUR) family protein involved in auxin response. In contrast, *Solyc02g084005.1* (1.31) and *Solyc03g082520.1* (2.79) are upregulated SAUR family proteins, also responding to auxin signaling. The gene *Solyc05g015880.3* (1.50), which encodes the protein LAZY1, is upregulated, and plays a crucial role in gravitropism by modulating auxin transport, affecting plant growth orientation. Additionally, *Solyc06g066770.1* (1.38) codes for an F-box domain-containing protein implicated in negative regulation of cytokinin signaling. Meanwhile, *Solyc07g061720.3* (−1.98) is downregulated and involved in gibberellin catabolism, influencing plant development. This pattern of upregulation and downregulation illustrates a dynamic hormonal regulatory network coordinating growth and environmental responses.

Three genes related to chloroplast function and primary metabolism showed differential expression. *Solyc06g082950.4*, encoding a Photosystem I subunit (PsaL), was downregulated (fold change: −1.20) and is associated with photosynthetic activity, specifically as part of the chloroplast thylakoid membrane and the Photosystem I reaction center. In contrast, *Solyc09g008660.3* was upregulated (fold change: 1.27) and encodes a CHUP1-like protein involved in chloroplast organization and associated with the chloroplast outer membrane. The gene *Solyc01g090710.3*, strongly upregulated (fold change: 6.81), encodes a malate dehydrogenase participating in multiple metabolic pathways including the TCA cycle, carbon fixation, and the glyoxylate cycle. This gene is involved in several key metabolic processes such as oxaloacetate and malate metabolism, suggesting a potential enhancement of energy production and carbon flow under the studied conditions.

Fruits

Figure 6c,d illustrates the transcriptomic response at 10 DAA in fruits under FR compared with the absence of FR at 1.5 , 24 , and 96 h. There is a relatively small number of DEGs at early time points, with minimal upregulation or downregulation at 1.5 and 24 h. However, at 96 h, a notable shift occurs, indicating a delayed but pronounced transcriptional response. Notably, the differential expression between sampling times—FR 24 h versus FR 1.5 h—revealed 1025 DEG, compared with only 494 DEG in fruits in the NO FR group. This pattern indicates a treatment-specific response over time: FR light induces a change in gene expression between time points, even if the expression levels at each individual time point are similar to those under NO FR light.

A total of 79 genes were differentially expressed in fruit when comparing FR to NO FR light treatments, with 48 of them being downregulated. This overall downregulation contrasts with the response observed in leaf tissue, where most DEGs were upregulated under the same conditions (Figure 6a). Notably, 68 of the 79 genes showed significant expression changes only at the 96 h time point, a trend that was also evident in the enrichment analysis, where the majority of DEGs were associated with the 96 h sampling (Figure 6b).

Contrary to the overall downregulation trend observed in fruit, six out of seven genes identified as TFs were upregulated. The exception was *Solyc02g062960.4*, a WRKY transcription factor, which was significantly downregulated, and only at 1.5 h. The first four transcription factors—*Solyc06g062460.3* (MYB), *Solyc01g090460.3* (NAC domain-containing), *Solyc06g060830.3* (bZIP), and *Solyc04g005800.3* (ERF)—were significantly upregulated at both 1.5 and 96 h, but not at 24 h. The remaining two—*Solyc05g053410.4* (bHLH) and Solyc06g008590.3 (HD-Zip)—were significantly upregulated only at 96 h (Figure S8).

At 96 h, several hormone-related genes were notably downregulated, particularly those associated with cytokinin and brassinosteroid biosynthesis pathways. Four genes—*Solyc05g053400.3*, *Solyc05g053120.1*, *Solyc07g043480.1*, and *Solyc11g066670.1*—are involved in zeatin biosynthesis, a key precursor of cytokinins, indicating suppression of cytokinin signaling at this late response stage.

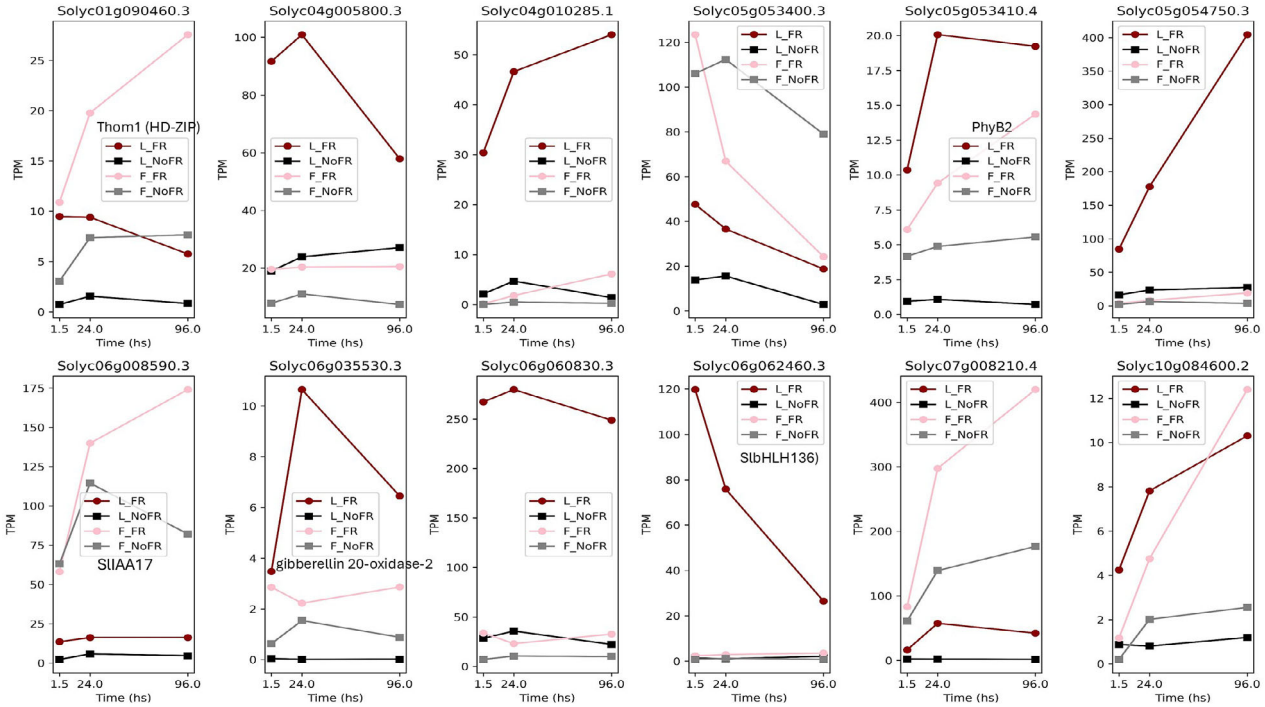

Figure 7. Temporal expression profiles of differentially expressed genes in leaf (L) and fruit (F) tissues under far-red (FR) and NO FR light conditions. Expression levels are represented as average transcripts per million (TPM) across three time points: 1.5, 24, and 96, with the first sampling point taken at 10 days after anthesis (DAA).

Additionally, *Solyc10g086500.1*, a gene directly related to brassinosteroid biosynthesis, was downregulated, along with several genes involved in steroid biosynthesis—precursors for brassinosteroids—including *Solyc01g091320.3*, *Solyc06g005750.3*, *Solyc02g086180.4*, and *Solyc02g069490.4*. In contrast, *Solyc06g035530.3*, annotated for gibberellin biosynthesis (GO:0009686) and involved in the diterpenoid biosynthesis KEGG pathway (00904), was upregulated, suggesting a specific activation of the gibberellin pathway despite the general downregulation of other hormone biosynthesis genes.

Fruits and Leaf transcriptomics

We analyzed the temporal expression profiles of the 12 DEGs in leaf and fruit tissues when comparing FR versus NO FR light conditions at three time points: 1.5, 24, and 96 h. The first sampling was performed at 10 DAA (Figure 7).

In leaf tissue, all 12 genes were significantly upregulated in FR-treated plants compared with controls at all time points. The strongest induction in leaves was observed for *Solyc06g035530.3* (gibberellin 20-oxidase-2) and *Solyc06g062460.3* (SlbHLH136), with log fold changes above 6 at 1.5 and 24 h, respectively (Figure 7). It is remarkably high for a transcription factor.

In fruit tissue, all genes were significantly upregulated at 96 h. Among these, *Solyc01g090460.3* (*Thom1*), *Solyc06g060830.3*, and *Solyc06g062460.3* also showed significant induction as early as 1.5 h, suggesting a rapid response to FR in fruit.

PhyB2 (*Solyc05g053410.4*) was strongly upregulated in leaves under FR light at all time points ($\log FC > 3.3$, $q < 10^{-53}$), while in fruit, it showed a moderate induction only at 4 days ($\log FC = 1.34$, $q = 1.05 \times 10^{-7}$). GO terms indicate roles in photoreceptor activity, signal transduction, and transcriptional regulation, supporting its function as a key light-responsive regulator.

Six of the genes—*Solyc05g054750.3*, *Solyc07g008210.4*, *Solyc10g084600.2*, *Solyc04g010285.1*, *Solyc04g005800.3*, and *Solyc06g060830.3*—were initially classified as unannotated in the Sol Genomics Network. However, when analyzing gene ontology (GO), KEGG, and PFAM data, we found evidence supporting functional roles for several of them.

Solyc06g060830.3 exhibited nuclear localization and DNA-binding transcription factor activity (GO:0005634, GO:0000981), supporting a regulatory role in light response. Similarly, *Solyc04g005800.3* was also predicted to localize to the nucleus and act as a transcription factor. *Solyc04g010285.1* carried the PF09713 domain, of unknown function but present in *Arabidopsis thaliana*, and was associated with the ribosome pathway in KEGG (03010).

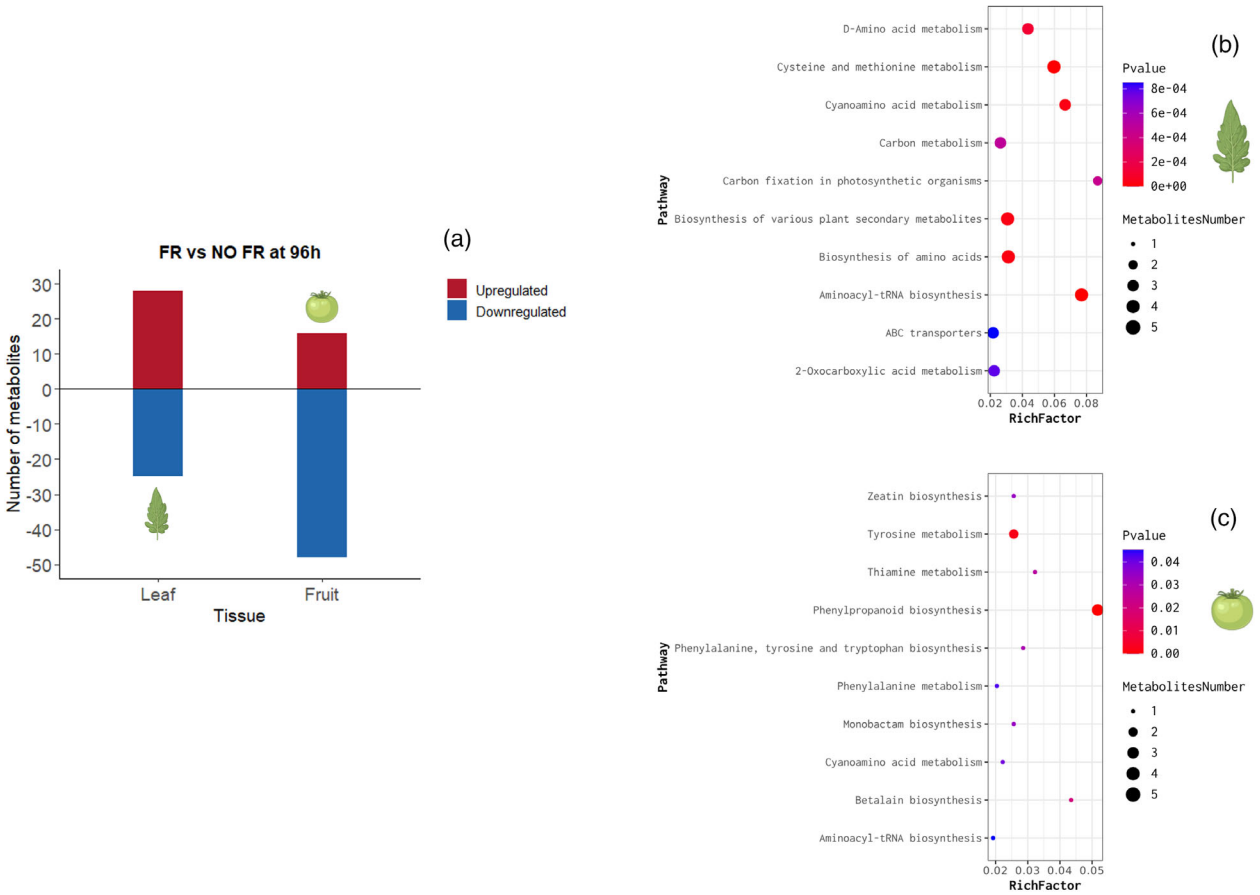

Figure 8. Metabolomic changes in response to far-red (FR) light at 96 h in leaves and fruits.
(a) Number of differentially accumulated metabolites (DAMs) in leaf and fruit tissues under FR versus NO FR conditions at 96 h. Red bars represent upregulated metabolites and blue bars represent downregulated metabolites.
(b) KEGG pathway enrichment analysis of DAMs in leaves.
(c) KEGG pathway enrichment in fruits. Dot size indicates the number of metabolites, and color represents the significance level (*P*-value).

Metabolomics on leaves and fruits

Metabolomic analysis was conducted in both fruits and leaves 10 DAA + 96 h after the exposure to FR, or NO FR. Similar to the response in transcriptomic analysis, there was a pronounced overall decrease in metabolite levels in fruit, which was not observed in leaves (Figure 8a).

In fruits, FR significantly enriched the metabolic pathways linked to aromatic amino acid metabolism and hormone-related processes. Notably, the biosynthesis of phenylpropanoids, tyrosine metabolism, and phenylalanine metabolism showed strong enrichment. This indicates activation of shikimate-derived secondary metabolism likely connected to ripening and stress signaling. The enrichment of zeatin biosynthesis suggests changes in cytokinin pathways, while the enrichment of cyanoamino acid metabolism reflects increased detoxification of cyanide, likely tied to higher ethylene production. The detection of metabolites associated with betalain biosynthesis reflects tyrosine-derived intermediates, highlighting the importance of aromatic amino acid flow (Figure 8c). These findings together show that metabolic pathways in fruits are reprogrammed, integrating hormonal regulation, nitrogen metabolism, and the production of specialized metabolites in response to FR treatment.

In leaves, FR caused broad metabolic changes focused on amino acid, sulfur, and carbon metabolism. The significant enrichment of D-amino acid metabolism, cysteine and methionine metabolism, and amino acid biosynthesis indicates improved use and redistribution of nitrogen and sulfur resources. The enrichment of aminoacyl-tRNA biosynthesis and ABC transporters suggests increased protein turnover and movement of metabolites, possibly supporting signaling throughout the plant. Cyanoamino acid metabolism was also enriched, aligning with stress-related cyanide detoxification. Concurrent changes in carbon metabolism and carbon fixation pathways point to

adjustments in primary photosynthetic outputs, while the enrichment of secondary metabolism pathways suggests a shift in metabolic activities toward signaling compounds or defense (Figure 8b). Overall, these results show that FR alters key metabolic networks in source tissues, likely influencing how fruit develops through long-distance metabolic signaling.

DISCUSSION

We investigated how FR light applied at different plant developmental stages affects tomato fruit growth and metabolism by combining physiological, metabolic, and transcriptomic analyses across both source and sink tissues. Previous studies showed that FR light enhances fruit biomass, alters sugar partitioning, and promotes stem elongation, often linking these outcomes to changes in source–sink dynamics or hormonal signaling (Ji et al., 2020; Pierik & Ballaré, 2021). Here, we dissected the temporal and tissue-specific effects of FR application. We revealed distinct developmental windows during which FR modulates plant architecture, sugar allocation, and gene expression. This allows us to identify not only what FR does, but also how and when it does so, advancing our understanding of light quality as a dynamic regulator of resource allocation in fruit-bearing crops.

Responses to far-red depend on plant development stage

Our results demonstrate that FR light modulates tomato plant architecture and fruit development in a stage-specific manner. Plants exposed to FR during the vegetative stage developed 60% larger leaf area than those exposed to FR from flowering to green fruit stage (Figure 1c), suggesting enhanced light interception. This likely boosted photoassimilate availability, explaining the higher total plant dry weight (Figure 1d), contributing to the formation of a greater number of fruits (Figure S3), although smaller in volume compared with treatment FR from flowering until green fruits (Figure 2b). These observations support the hypothesis that FR exposure during the vegetative phase shifts resource allocation toward leaf expansion, enhancing source strength and promoting early reproductive growth.

FR can enhance both source strength, by increasing the photosynthesis rate (Zhen & Bugbee, 2020), and fruit sink strength (Ji et al., 2020). Thus, the effect of FR application from vegetative until flowering on yield can be attributed to enhanced source strength, leading to greater assimilate availability during fruit development. Furthermore, the promotion of yield by applying FR from flowering until full-grown green fruits may result from increased sink strength in developing fruits, enhancing their capacity to attract and utilize assimilates (Figure 1e).

FR light during the vegetative stage enhances leaf sugar pools via a jasmonic acid–dependent pathway (Courbier et al., 2020), whereas FR exposure during fruit development promotes sugar allocation to fruits by upregulating sugar transporter genes and increasing fruit sink strength (Ji et al., 2020). In our study, starch content in fruits at 35 DAA was highest under FR treatment from flowering until full-grown green fruits, followed by FR applied throughout the entire growth cycle (Figure 3b). The comparatively lower starch content in the latter treatment likely reflects a more advanced fruit developmental stage, as indicated by earlier color change (Figure 2e). Since starch is degraded into soluble sugars during maturation, and sugars concurrently accumulate via phloem import (Braun, 2022), the elevated sugar content under continuous FR may result from the combined effects of enhanced source capacity, increased sink activity, and residual starch reserves. In contrast, the slightly lower sugar content observed under FR from flowering to the green fruit stage likely reflects a sink-driven enhancement without a prior increase in source metabolism (Figure 2d).

Plant height responses, also reflect the stage-specific action of FR, with the greatest elongation observed when FR was applied during the vegetative phase or continuously (Figure 1b). In contrast, FR exposure from flowering to the full-grown green fruit stage did not promote elongation, likely due to assimilate allocation toward reproductive sinks. This aligns with prior findings (Ji et al., 2021; Kalaitzoglou et al., 2019; Meijer et al., 2022) and suggests that post-flowering FR application enhances fruit quality without compromising compact plant architecture, an advantage for controlled environment and high-density cultivation.

Far-red stimulates both pericarp cell layers and cell volume

Fruit size is largely determined by cell division and expansion in the pericarp, with cell size positively correlated with fruit weight (Ariizumi et al., 2013). Interestingly, we found that FR application affects both the number of cell layers (cell division) and cell volume (cell expansion) depending on the developmental phase during which FR is applied (Figure 4c,d). The present findings align with the established developmental timeline in cherry tomato pericarp. FR application from pre-anthesis to 7 DAA increased mesocarp cell layers (Figure 4c), consistent with the cell division phase, which concludes by around 10 DAA (Renaudin et al., 2017). This suggests that early FR enhances mitotic activity. In contrast, FR applied from 7 to 36 DAA (post-mitotic phase) did not affect cell layer number but significantly increased mesocarp cell volume (Figure 4c,d), indicating promotion of cell expansion rather than proliferation.

To uncover early molecular changes leading to the fruit phenotype observed at 35 DAA, RNA-seq was conducted on fruits at 10 DAA and at 1.5 , 24 , and 96 h after FR

application. We observed distinct hormone-related transcriptional responses in both leaves and fruits. In leaves, the earliest time point (DAA10 + 1.5 h) revealed GO terms related to hormone pathways: auxin, cytokinin, brassinosteroid, and gibberellin, which were present in both upregulated and downregulated gene groups. In fruit tissue, the strongest hormone-related transcriptional changes were observed at DAA10 + 96 h, with GO terms related to auxins, gibberellins, and brassinosteroids.

Fruit growth promotion by far-red is associated with increased auxin signaling

The significant FR-induced increase in cell division (Figure 4c) was accompanied by elevated expression of *Sl-IAA17* (*Solyc06g008590*), a transcriptional regulator, in both fruits (10 DAA + 24 h) and leaves (10 DAA + 1.5 h and 10 DAA + 96 h). Although silencing of *Sl-IAA17* has previously been linked to larger fruits and thicker pericarps due to enhanced cell endoreduplication (Su et al., 2014), its increased expression in our study may reflect feedback regulation within the auxin signaling network.

Aux/IAA genes, including *IAA17*, are transcriptionally induced by auxin as part of a negative feedback loop that fine-tunes auxin responses (Perrot-Rechenmann, 2010; Wang & Ruan, 2013). Consistent with this, our transcriptome analysis showed strong enrichment of the GO term "auxin response" at 10 DAA + 1.5 h, along with upregulation of several auxin-related genes in leaves (*Solyc01g110730*, *SAUR10* [*Solyc01g110710*], *SAUR11* [*Solyc01g110770*], *SAUR47* [*Solyc04g053000*], *Solyc01g110790*, *YUC9* [*Solyc06g083700*], *GH3.8* [*Solyc08g068490*]) (Figures S4 and S5). These transcriptional changes indicate enhanced auxin activity under FR treatment, which is in line with previous studies (Li et al., 2012; Pierik & Ballaré, 2021).

Because auxin can be transported from source tissues (leaves) to sink tissues (developing fruits) (Park et al., 2017; Zažímalová et al., 2010), increased auxin-related transcription in leaves may have contributed to elevated auxin signaling in fruits. Although auxin concentration was not directly measured, the coordinated upregulation of auxin biosynthetic and responsive genes suggests enhanced auxin signaling, likely promoting the observed stimulation of cell division in fruits (Figure 4).

Overall, our findings support a model in which FR enhances auxin biosynthesis and transport, thereby promoting fruit growth. The increased *Sl-IAA17* expression may act as a compensatory mechanism to fine-tune this increased auxin response during fruit development.

Gibberellin-related gene regulation under far-red

Direct connection between the auxin and gibberellin (GA) signaling channels plays a crucial role in controlling the initiation and growth of tomato fruit (Hu et al., 2018). Additionally, GA may play a negative role in tomato fruit ripening in an ethylene-dependent manner (Li et al., 2019) highlighting the dynamic and time-dependent nature of hormone responses during fruit development.

We found that *GA 20-oxidase* (*Solyc06g035530*), a key enzyme in gibberellin biosynthesis, was significantly upregulated by FR in both fruits (10 DAA + 96 h) and leaves (from 10 DAA + 1.5 h onwards; Figure 7). Overexpression of *GA 20-oxidase* is known to increase fruit size by elevating gibberellin levels during early development (Serrani, Fos, et al., 2007; Serrani, Sanjuán, et al., 2007; García-Hurtado et al., 2012). Both gibberellin (GA) and auxin contribute to pericarp thickening, but through different mechanisms: auxin mainly promotes cell division (increasing the number of cell layers), whereas GA enhances cell expansion, possibly by influencing cell ploidy (Serrani, Fos, et al., 2007; Serrani, Sanjuán, et al., 2007). This distinction helps explain our observations. FR applied from the vegetative stage until flowering increased the number of mesocarp cell layers, likely due to elevated auxin activity during the active division phase (De Jong et al., 2015), consistent with the induction of the auxin-related gene (*Sl-IAA17* [*Solyc06g008590*]) in fruits at 10 DAA + 24 h. In contrast, FR applied from flowering until the full-grown green fruit stage enlarged mesocarp cells, consistent with the upregulation of the GA-related gene (*GA 20-oxidase* [*Solyc06g035530*]) in fruits at 10 DAA + 96 h. When FR was terminated before the expansion phase (FR from vegetative until flowering), cell enlargement was limited. However, FR exposure from flowering onward promoted larger cells once cell division was complete (Figure 4c,d). Future studies that directly quantify hormone levels would help clarify the contributions of auxin and GA to these FR-induced developmental changes.

In addition to *GA 20-oxidase*, the gene *SlGASA1*, also known as *GAST1* (*Gibberellin Stimulated Transcript 1* – *Solyc02g089350*), was found to be upregulated in leaves at 10 DAA + 1.5 h by FR (Figure S6). However, its expression was not significantly different at 10 DAA + 24 h and 10 DAA + 96 h, and no significant changes at the expression level were observed in fruit at any time point. Interestingly, overexpressing *SlGASA1* using a ripening-specific promoter delayed the onset of fruit ripening, whereas *SlGASA1*-knockdown fruits displayed accelerated ripening (Su et al., 2023). Since *SlGASA1* is downregulated in fruit at later stages (breaker stage), (Su et al., 2023), it is possible that our transcriptomic assay did not capture the variation in the expression in fruit. Regarding gene expression in leaves, there is not much information about the impact of this gene in tomato leaves; however, Sun et al., 2013, found that in Arabidopsis, a homologous gene, *GASA14*, promotes cell expansion and leaf size.

Furthermore, we found the gene *PRE1* (Solyc06g 062460) to be significantly upregulated with the addition of

FR in both fruits and leaves—with leaves having a very strong increase in expression level at DAA10 + 1.5 h (Fig ure 7). This is in agreement with *PRE*-upregulation observed under low R:FR (Kohnen et al., 2016). In *Arabidopsis*, overexpression of *PRE1* resulted in a phenotype associated with an enhanced GA response (Lee et al., 2006). When *PRE2* was silenced in tomato, a strong reduction of fruit size, pericarp thickness, and cell size in fruit mesocarp was observed, while it was also shown that *SlPRE2* was gibberellic acid-inducible (Zhu et al., 2019).

These three genes (*GA 20-oxidase*, *SlGASA1, PRE1*) displayed a GA-related transcriptional response in leaves at DAA10 + 1.5 h. Of these, two also responded in fruits at 10 DAA + 96 h, suggesting that leaves are the primary site of perception following the light shift. This temporal pattern is further supported by the overall number of DEGs, which is markedly higher in leaves than in fruits at both 10 DAA + 1.5 h and 10 DAA + 24 h (Figure 6a,c). These findings suggest that signal transduction is initiated in the leaves and may subsequently influence gene expression in the fruit.

It is plausible that signaling molecules originating in the leaves, such as GA or upstream regulators, are transported to the fruit. GA, once synthesized, can act locally or be translocated to distant organs via the vascular system, particularly the phloem, to mediate systemic developmental responses (Lucas et al., 2013; Lacombe & Achard, 2016). For example, in *Arabidopsis thaliana*, GA precursors such as GA have been shown to move from the shoots to the roots, where they regulate root growth (Binenbaum et al., 2023). A similar long-distance signaling mechanism may underlie the leaf-to-fruit communication observed here.

Alternative to GA movement, it was recently revealed that *PRE1-5* can move between root-tip cells in *Arabidopsis* (Lu et al., 2018). Given that the *PREs* are small bHLHs (92–94 amino acids) and lack a typical DNA-binding domain (Hyun & Lee, 2006; Mara et al., 2010), they are structurally compatible with movement. However, whether *PREs* are capable of long-distance movements, specifically from leaves to fruits, remains unexplored.

Furthermore, at 10 DAA + 96 h, both the expression of the cytokinin-related genes f(*Solyc05g053400.3*, *Solyc05g053120.1*, *Solyc07g043480.1*, and *Solyc11g066670.1*) and the level of zeatin hormone were downregulated in fruits treated with FR (Figure 8c). Cytokinins are key regulators of cell division during the early stages of fruit development, promoting mitotic activity in the pericarp (Gan et al., 2022; Kumar et al., 2013; Matsuo et al., 2012). Their decline at 10 DAA + 96 h suggests that the intensive cell division phase is coming to an end, and the fruit is entering the cell expansion phase, where growth relies primarily on cell enlargement rather than cell proliferation (Kumar et al., 2013). Gibberellins, which become more active during the expansion phase, promote cell wall loosening and vacuolar enlargement to drive fruit growth (Serrani, Fos, et al., 2007; Serrani, Sanjuán, et al., 2007). Together, these changes indicate a developmental shift from cell division to gibberellin-driven cell expansion in fruits at 10 DAA + 96 h.

Transcription factors response to far-red

Among the genes analyzed, five showed significant upregulation in the fruit at different time points. Four genes—*Solyc01g090460*, *Solyc04g005800*, *Solyc06g060830*, and *Solyc06g062460*—exhibited a consistent pattern of expression at both 10 DAA + 1.5 h and 10 DAA + 96 h, indicating early and late transcriptional activity in response to FR. Interestingly, these genes were also upregulated in leaves at the first time point (Figure 7).

THOM1 (Solyc01g090460) is a homeobox-containing transcription factor that was found to play a key role in tissue regeneration during graft formation in tomato (Thomas et al., 2022). Specifically, *THOM1* was identified as a marker of meristematic activity and was specifically expressed in regenerating pith cells at the graft junction. It operates within a transcriptional module that activates genes involved in cell wall remodeling and proliferation, such as xyloglucan endotransglucosylase/hydrolases (XTHs). In the context of our experiment, the FR-induced increased expression of *THOM1* in tomato fruit suggests a potential role in promoting cell proliferation within pericarp cells.

SlHZ24 (*Solyc04g005800*) is known to promote ascorbate (AsA) biosynthesis, thereby enhancing oxidative stress tolerance in leaves (Hu et al., 2016). In that study, expression of this gene was detected in immature fruit but not in mature green, breaker, or red-ripe fruit stages. Given the crucial role of ascorbate during fruit development, it is plausible that this transcription factor may have a similar function in both fruit and leaves. However, due to pleiotropic nature of TFs, the precise role of *SlHZ24* in tomato fruit remains unclear.

Similarly, *Solyc06g060830*, the putative tomato *HB2*, is proposed to function as a transcription factor involved in the negative regulation of cell elongation and specific cell proliferation processes, such as lateral root formation and secondary vascular growth (Ohgishi et al., 2001; Schena et al., 1993). It is also implicated in mediating R:FR light responses affecting leaf cell expansion during shading (Steindler et al., 1999). However, there are no studies on fruit tissues, and its role in fruit development has yet to be validated.

Finally, for *Solyc06g062460*, despite its classification as a bHLH transcription factor—a family known to play key regulatory roles in plant development, there is only expression data available. Together, these findings highlight the need for further functional studies of these TFs

in fruit tissue and their involvement in shaping fruit size. Going beyond the fruit and considering their delayed response to light, we also evaluated TFs with rapid responses in leaves. Among these, *TCP20* (Solyc08g 080150) stands out with a higher FoldChange at 10 DAA + 1.5 h (Figure S6).

TCP proteins are TFs that perform critical functions in plant growth and development. Despite their acknowledged importance in overall plant development, these TFs' precise involvement in fruit growth remains largely unknown. The TCP family is divided into two subfamilies: Class I (TCP-P subfamily) and Class II (TCP-C subfamily) (Navaud et al., 2007). *TCP20* is classified in Class I which is known to promote cell proliferation and plant growth (Li et al., 2005; Martín-Trillo & Cubas, 2010). More recent studies have found that *SlTCP12*, *SlTCP25*, and *SlTCP18* are regulated by ripening inhibitor, colorless non-ripening, and APETALA2a proteins, suggesting that *TCP* TFs contribute to the development or ripening of tomato fruits (Parapunova et al., 2014). A recent study showed that *TCP20* was upregulated in low R:FR conditions in both the whole tomato internode and the central cylinder, further supporting a role in the regulation of cell size (Li et al., 2025).

Temporal and systemic regulation of FR-induced faster fruit development from anthesis to ripening in tomato

FR treatment triggered early transcriptional responses in leaves, notably the rapid induction of *NAC6* (*Solyc02g 061780*) within 1.5 h of exposure (Figure S6). *NAC6*, a *NAC* transcription factor regulating carotenoid biosynthesis and ABA signaling (Forlani et al., 2021; Jian et al., 2021; Kou et al., 2021; Zhu et al., 2014), positively influences ripening, as shown by *SlNAC6* overexpression, which accelerates fruit maturation (Jian et al., 2021). Concurrently, *notabilis* (*Solyc07g056570*), encoding *NCED1*, an ABA biosynthesis enzyme, was strongly upregulated at 1.5 h (Figure S6). In tomato, *NCED1* is critical for ABA accumulation and ripening progression (Ji et al., 2014; Sun et al., 2012). Additionally, *ACS3* (*Solyc02g091990*), a key ethylene biosynthesis gene, was significantly induced in leaves, suggesting early activation of ethylene signaling (Chen et al., 2022) (Fig ure S5). Collectively, these data indicate that FR rapidly activates *NAC6, NCED1,* and *ACS3* in leaves, promoting ABA and ethylene pathways known to coordinate ripening onset.

Phenotypic consequences of FR exposure were evident at the fruit level: FR application from flowering until the full-grown green fruits (7–38 DAA) accelerated ripening by 3 days compared with NO FR (Figure 2e). In contrast, FR applied after 38 DAA had no effect on fruit ripening. After 38 DAA, endogenous hormonal and transcriptional programs dominate, and ethylene production reaches its climacteric peak (Zhang et al., 2020), rendering external stimulation ineffective. Thus, the capacity of FR to accelerate ripening is temporally restricted to the pre-breaker phase, emphasizing the importance of treatment timing.

At the fruit level, metabolomic analysis at 10 DAA + 96 h post-treatment revealed phenylpropanoid pathway enrichment (Figure 8c), indicating a shift toward ripening-associated secondary metabolism, including flavonoids and phenolic acids involved in pigmentation, cell wall remodeling, and antioxidant defense (Singh et al., 2010). The sequential occurrence of early transcriptional changes in leaves and subsequent metabolic shifts in fruits supports the existence of systemic signaling from vegetative to reproductive tissues in response to FR. While the mechanistic link between vegetative and reproductive tissues remains to be elucidated, these observations align with a model in which FR triggers systemic regulation of ripening processes during early fruit development.

CONCLUSIONS

Our results demonstrate that FR exerts stage-dependent effects on tomato development, differentially influencing source (leaves) and sink (fruits) tissues. FR application during the period from flowering to the green fruit stage had the strongest impact, markedly enhancing fruit growth, modifying fruit anatomy, and affecting ripening. By applying FR at distinct developmental phases, we show that the timing of light exposure determines whether FR enhances leaf area or promotes cell division and expansion in developing fruits. Furthermore, the earlier transcriptional responses to FR in leaves compared with fruits indicate that vegetative tissues perceive and respond to FR first. This temporal pattern suggests that signaling from leaves may subsequently influence fruit development, potentially through a mobile factor or systemic signal. Overall, these insights into developmental phase-specific FR effects open new avenues for optimizing crop yield and quality through precise temporal and spatial manipulation of light environments.

MATERIALS AND METHODS

Plant material and growth conditions

Dwarf tomato seeds (*Solanum lycopersicum* cv. Heartbreakers Vita; Prudac, The Netherlands) were sown on September 5, 2023 in stonewool plugs and germinated in a growth chamber at Wageningen University & Research (The Netherlands). Two weeks after germination, seedlings were transplanted into 10 × 10 × 6.5 cm stonewool blocks (Grodan, Roermond, The Netherlands). On October 1, 2023, uniform plants were selected and distributed across 10 growth chamber compartments, each containing six plants for measurements. Growth conditions were: photosynthetically active radiation (PAR, 400–700 nm) of 200 $\mu mol\ m^{-2}\ s^{-1}$ with a 16 h photoperiod; spectrum composition of 19.04% blue (400–500 nm), 31.82% green (500–600 nm), and 26.48% red (600–700 nm); and far-red (FR) supplementation in four of five

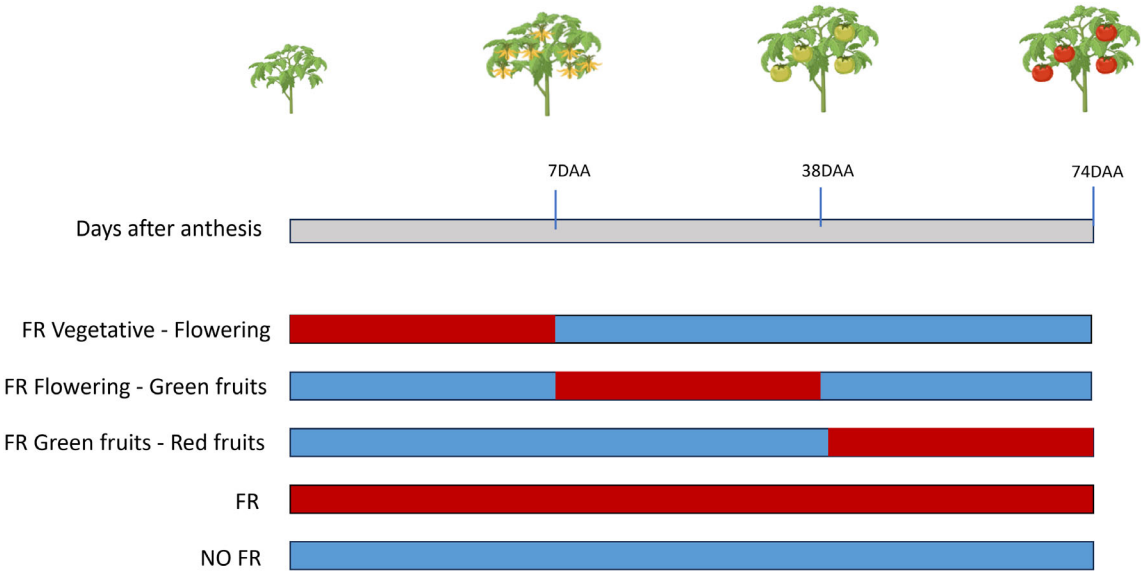

Figure 9. Schematic representation of the light treatments applied in the present study.
All plants received 200 μmol m^{-2} s^{-1} PAR light. Additional 50 μmol m^{-2} s^{-1} was applied throughout the entire growth cycle (FR) or not at all (NO FR) or during a specific developmental phase. The FR vegetative–flowering treatment received FR exclusively during the vegetative phase up to flowering (7 DAA). In the FR Flowering–Green Fruits treatment, FR was applied from flowering (7 DAA) until the development of full-grown green fruits (38 DAA). The FR Green Fruits–Red Fruits treatment received FR from the full-grown green fruit stage until the red fruit stage.

treatments (details below). Temperature and relative humidity were maintained at 22 ± 0.5/19 ± 0.5°C (day/night) and 65%, respectively. Plants were grown on ebb–flood tables and irrigated twice daily (3 min) with nutrient solution (EC 2.1 dS m^{-1}, pH 5.5) containing 1.2 mM NH^+, 7.2 mM K^+, 4.0 mM Ca^{2+}, 1.8 mM Mg^{2+}, 12.4 mM NO^-, 3.3 mM SO^{2-}, 1.0 mM PO^{2-}, 35 μM Fe^{3+}, 8.0 μM Mn^{2+}, 5.0 μM Zn^{2+}, 20 μM B, 0.5 μM Cu^{2+}, and 0.5 μM MoO^{2-}. The EC and pH were monitored biweekly. Flowers were manually pollinated three times per week using a Vibri Vario electronic bee (Royal Brinkman, 's-Gravenzande, The Netherlands).

Far-red treatments

Three batches of plants, sown on the same date, were used for measurements at different time points to investigate the effects of FR applied at different plant developmental stages on tomato growth, total fruit fresh weight, and physiology. These included:

1. A long-term development and growth study up to 74 days after anthesis (DAA)
2. A study focused on a critical developmental stage at 35 DAA
3. A transcriptomic (RNA-sequence) and metabolomic analysis at 10 DAA to identify early molecular responses triggered by FR.

Long-term developmental and growth study (up to 74 DAA)

To evaluate the impact of additional FR (50 μmol m^{-2} s^{-1}) across the plant's life cycle, plants were assigned to five treatments of six plants each, each corresponding to the addition of FR at distinct plant developmental stages (Figure 9). Each treatment was randomly assigned to two of the 10 compartments. The developmental stages in which FR was applied were from vegetative until anthesis of first flowers (7 DAA), from flowering until first full-grown green fruits (38 DAA), from fully grown green fruits until red fruits (74 DAA), also FR was applied throughout the entire growth cycle, and absence of FR (Figure 1). The duration of FR was equal in all FR treatments, and that was 30–36 days. Thus, we kept the duration and intensity of FR the same and we changed only the developmental stage in which FR was applied.

Three plants out of each compartment were designated for long-term measurements collected at the end of the growth cycle (74 DAA), while the other three plants were used for the analysis at 35 DAA. For the analysis at 35 DAA, only the fruits required for the measurements described below, were harvested. The plants themselves remained in place to preserve planting density, light distribution, and overall microclimatic conditions within each compartment.

Growth parameters

The number of fruits with a diameter of more than 5 mm and the number of trusses was registered once per week over a period of 6 weeks. To determine fruit growth as a function of time, non-destructive measurements of fruit height (h) and fruit diameter (d) were conducted on the second and third fruit of the first truss of each plant once per week over a period of 6 weeks. The formula of Li et al. (2015) was used to calculate fruit volume:

$$v = \frac{4}{3}\pi\left(\frac{d}{2}\right)^2\frac{h}{2}$$

Fruit color measurements

Tomato fruit skin color development was monitored over time using a portable colorimeter (CR-400, Konica Minolta, Tokyo, Japan). Color measurements were conducted at 40, 45, 47, 50, 53, and 57 DAA. The initial time point (40 DAA) corresponded to the mature green stage, and measurements continued until

fruits reached the red ripe stage, after which they were harvested. Measurements were performed on the second and third fruit of the first truss on each plant. For each fruit, four measurements were taken around the equatorial region, and the average of these readings was used to calculate a mean color value per fruit.

Among the colorimetric parameters recorded (L^*, a^*, b^*), the a^* value—indicative of the green-to-red transition—was used to quantitatively represent fruit color change over time.

Destructive measurements

Fruits were harvested when ripe from 57DAA until the final harvest (74 DAA). The number of fruits was determined, and total fruit fresh weight (FW) was measured. Fruit dry weight was determined after drying in a ventilated oven at 70°C for 24 h and then at 105°C for 75 h. At the end of the cultivation cycle (74 DAA) plant height was recorded, and stems and leaves were separately dried at 70°C for 24 h followed by 105°C for 75 h.

Carbohydrate analysis

To ensure that fruits used for carbohydrate analysis were at the same maturation stage across all treatments, fruit skin color was monitored using a portable colorimeter (CR-400, Konica Minolta, Tokyo, Japan). Fruits were harvested for analysis when the a^* value reached 25, a threshold corresponding to the red ripe stage. This approach allowed for standardization of physiological maturity, regardless of differences in ripening time among treatments.

From each plant, the second and third fruit from the first truss were harvested and quickly sliced into two halves. One half was immediately frozen in liquid nitrogen for later use and the other half was weighed for FW before being transferred to a ventilated oven for drying (24 h at 70°C and then 75 h at 105°C), after which the dry weight was measured.

Frozen tissue of each individual sample was ground mechanically into fine powder with liquid nitrogen. Then, equal weights of powdered tissues harvested from positions two and three from the same plant were pooled into one sample and mixed well. In total, there were six samples per treatment. Glucose, fructose, and sucrose concentrations were measured as described by Plantenga et al. (2019) with an adaptation that 300 mg ground frozen fresh material from each pooled sample was weighed and mixed with 5 mL of 85% ethanol in a shaking water bath for 20 min at 80°C. After centrifugation at 8500 *g* for 5 min, 1 mL of the supernatant containing soluble sugars was vacuum dried using a Savant SpeedVac rotary evaporator (SPD2010; Thermo Fisher Scientific, Waltham, MA, USA) and then dissolved in 1 mL Milli-Q water and diluted 50× for analysis of soluble sugars. Sucrose, fructose, and glucose quantification was conducted using a high-performance ion chromatograph (ICS-5000; Thermo Fisher Scientific) with an anion CarboPac 2 × 250 mm exchange column (PA1; Thermo Fisher Scientific) at 25°C with 100 nM NaOH as eluent at the flow rate of 0.25 mL min^{-1}. Pulsed amperometry was used for detection and Chromeleon (Thermo Fisher Scientific) was used for analysis of the chromatograms and quantification of sugar concentrations.

Study focused on the developmental stage 35 DAA

For plants used to study the effect of FR at 35 DAA, exactly the same experimental set-up was used with the only difference that the treatment of FR applied from full-grown green fruits until red fruits was not included. Individual fruit FW from the second and third fruit of the first truss from all plants was recorded at 35 DAA. Then the fruits were cut in half, and one half was used for carbohydrate and starch analysis while the other half was used for pericarp cell histology. For carbohydrates the procedure described above was followed. The extra step that happened here was that the remaining pellet after sugar extraction was used for starch determination. After discarding the supernatant that contained the soluble sugars, the remaining pellet was washed three times with 80% ethanol, each time followed by 5 min centrifugation and removal of the supernatant. The remaining pellet was dried for 20 min in a SpeedVac rotary evaporator and resuspended in 2 mL 1 mg ml^{-1} thermostable α-amylase solution (Serva Electrophoresis, Heidelberg, Germany) and incubated for 30 min at 90°C. Then, 1 mL of 0.5 mg ml^{-1} amyloglucosidase (10 115; Sigma-Aldrich) in 50 mM citrate buffer (pH 4.6) was added and the mixture incubated for 15 min at 60°C so that the starch in the sample was converted into glucose. After centrifugation for 5 min at 8500 g, 1 mL of the supernatant was diluted 50× and was used for quantification of glucose content as described above.

Pericarp cell histology

The other half of the fruit was used for pericarp cell histology. Samples fixed in a solution containing ethanol (96%), acetic acid, formaldehyde (37%), and Milli-Q water, and later embedded following the Technovit protocol (Kulzer, Wehreim, Germany) as described by Fanwoua et al. (2012) and Okello et al. (2015). Slides (3 μm thick) were prepared, stained using 1% toluidine blue dye. Images were observed using a microscope and nis-elements software (Nikon Instruments, New York NY), and were analyzed using ImageJ software (National Institutes of Health, Rockville, MD). Pericarp thickness, the number of cell layers, longitudinal cell diameter, mean cell volume, tissue volume, tissue cell number and weighted pericarp cell volume were determined as described by Fanwoua et al. (2012) and Okello et al. (2015).

RNA extraction and quality assessment

To capture the earliest transcriptional and metabolic responses underlying FR-mediated effects on tomato development, leaf and fruit tissues were collected from five biological replicates per organ at the following time points: 10 DAA + 1.5 h (h), 10 DAA +24 h, 10 DAA + 96 h after the exposure, or not, to FR and immediately flash-frozen in liquid nitrogen. Sampling at earlier stages was not feasible due to the very small fruit size, which would not provide sufficient biological material for reliable RNA and metabolite extraction. Samples were stored at −80°C before RNA extraction.

Total RNA was extracted using a modified CTAB protocol (Bio Basic, Toronto, Canada), optimized for high polysaccharide and polyphenol content in plant tissues. Briefly, frozen tissue was ground in liquid nitrogen and homogenized in 1.5 mL pre-heated CTAB lysis buffer (supplemented with 2% β-mercaptoethanol) at 65°C. Homogenates were incubated for 15 min at 65°C, cooled to room temperature, and centrifuged at 12000 × ***g*** for 5 min at 4°C. The supernatant was transferred to a new tube, mixed with 0.2 volumes of chloroform:isoamyl alcohol (24:1, v/v), and centrifuged at 12000 × ***g*** for 10 min at 4°C. The aqueous phase was sequentially extracted with phenol:chloroform:isoamyl alcohol (25:24:1, v/v/v), followed by chloroform:isoamyl alcohol (24:1, v/v), each with centrifugation at 12000 × ***g*** for 10 min at 4°C. RNA was precipitated by adding 2/3 volume of isopropanol and incubating at −20°C for 2 h, followed by centrifugation at 12000 × g for 20 min at

4°C. The pellet was washed with 75% ethanol, centrifuged at 17500 × g for 3 min at 4°C, air-dried for 3–5 min, and resuspended in DEPC-treated RNase-free water. RNA concentration and integrity were assessed using a Fragment Analyzer system (Agilent Technologies, CA, USA).

Library construction and RNA sequencing

Strand-specific mRNA libraries were constructed using the Optimal Dual-mode mRNA Library Prep Kit (BGI-Shenzhen, China). Total RNA was denatured and polyadenylated mRNA was enriched using oligo(dT)-coupled magnetic beads. Enriched mRNA was fragmented and reverse-transcribed with random hexamer primers to synthesize first-strand cDNA. Second-strand synthesis was performed using dUTP in place of dTTP. The resulting double-stranded cDNA underwent end repair, A-tailing, and adapter ligation. Libraries were amplified via PCR and subjected to quality control. Single-stranded circular DNA libraries were generated by denaturation and ligation, followed by exonuclease digestion of residual linear DNA. DNA nanoballs (DNBs) were produced by rolling circle amplification using phi29 DNA polymerase and loaded onto a patterned nanoarray. Paired-end 150 bp sequencing was conducted on the BGISEQ-500 G400 platform (BGI-Shenzhen, China).

Bioinformatic analysis

Raw sequencing data were processed using SOAPnuke to remove adapter-containing reads, low-quality reads (>20% bases with $Q \leq 15$), and reads with >5% ambiguous nucleotides. Clean reads were aligned to the *S. lycopersicum* reference genome using HISAT2 for structural variant and splice junction identification. Fusion gene detection and differential splicing analysis were performed with Ericscript (v0.5.5) and rMATS (v4.1.2), respectively. Transcript identification was achieved via Bowtie2 alignment against a combined reference set of known and novel, coding and non-coding transcripts. Gene-level expression was quantified using RSEM (v1.3.1). Differential gene expression was determined using DESeq2 (v1.34.0), DEGseq (v1.48.0), or PoissonDis, with statistical significance thresholds set at $Q \leq 0.05$ or FDR ≤0.001. GO and Kyoto Encyclopedia of Genes and Genomes (KEGG) enrichment analyses were conducted via the Hypergeometric test using Phyper, with multiple testing correction applied ($Q \leq 0.05$). Heatmaps were visualized using the R package *pheatmap* (v1.0.12). Analyses were conducted on the Dr.TOM II Multi-omics Data Mining platform.

Metabolomic profiling and analysis

Sample preparation and metabolite extraction

Leaf and fruit samples (five biological replicates each) were collected at 10 DAA + 96 h, flash-frozen in liquid nitrogen, and ground into fine powder. Approximately, 50 mg of each sample was shipped on dry ice to BGI (Shenzhen, China) for untargeted metabolomic profiling. Metabolite extraction was performed by suspending each powdered sample in 800 μL pre-cooled methanol: water (7:3, v/v) extraction buffer supplemented with 20 μL of internal standard mix (d -leucine, ^{13}C -phenylalanine, d -tryptophan, ^{13}C -progesterone). Samples were homogenized at 50 Hz for 10 min, ultrasonicated (4 °C, 30 min), incubated at −20 °C for 1 h, and centrifuged (14 000 rpm for 15 min at 4 °C). Supernatant (600 μL) was filtered through a 0.22 μm membrane and transferred to LC–MS vials. Quality control (QC) samples were prepared by pooling equal aliquots from each extract to assess analytical stability and reproducibility.

UPLC–MS/MS analysis and data acquisition

Chromatographic separation and mass spectrometry were performed using ultra-performance liquid chromatography (UPLC) coupled to a high-resolution tandem mass spectrometer (Thermo Fisher Scientific, USA). All reagents used (methanol, acetonitrile, formic acid, and ammonium formate) were LC–MS grade. The system was calibrated and tuned for high sensitivity and resolution. Instrument parameters, including retention time window (±0.2 min), precursor ion mass accuracy (<5 ppm), and fragment mass deviation (<10 ppm), were optimized to ensure high-confidence metabolite detection.

Peak detection and metabolite identification

Raw mass spectrometric data were processed using *Compound Discoverer* (v3.3; Thermo Fisher Scientific), integrating information from multiple databases including BMDB (BGI Metabolome Database), mzCloud, and ChemSpider for metabolite annotation. A final metabolite matrix comprising peak area and identification data was generated for downstream analyses. Functional annotation of identified metabolites was conducted using the KEGG and Human Metabolome Database (HMDB), enabling classification into metabolic pathways and biological categories.

Data preprocessing and normalization

The metabolite data matrix was imported into MetaX for normalization and QC. Data were normalized using probabilistic quotient normalization (PQN) to correct for dilution variability, and batch effects were adjusted using QC-based robust LOESS signal correction (QC-RLSC). Features with >30% coefficient of variation in QC samples were excluded to ensure data quality.

Experimental set-up and statistical analysis

Each light treatment was applied in two independent compartments; data were analyzed with one-way ANOVA, with FR light being the treatment factor. For all analyses RStudio (R version 4.3.2) was used. Post-hoc analyses were performed using the '*emmeans*' package to perform pairwise comparisons of treatment means applying Tukey's honest significance test. For all statistical tests, probability level α was 0.05. To generate plots, the '*ggplot2*' package was used.

Principal component analysis (PCA) was employed as an unsupervised method to assess sample clustering, variation, and potential outliers. Metabolite features were log -transformed and Pareto-scaled prior to analysis. Supervised discrimination was performed using partial least squares-discriminant analysis (PLS-DA) and orthogonal PLS-DA (OPLS-DA) with sevenfold cross-validation. Variable importance in projection (VIP) scores >1 were used to identify discriminatory metabolites between leaf and fruit samples.

ACKNOWLEDGMENTS

We are grateful to the Unifarm Klima staff, namely, Gerrit Stuunenberg, David Brink, and Dieke Smit for the excellent support. This work was supported by Blue Skies Discovery (https://www.linkedin.com/company/blueskiesdiscovery/about/).

CONFLICT OF INTEREST

The authors declare that the research was conducted in the absence of any commercial or financial relationships that could be construed as a potential conflict of interest.

DATA AVAILABILITY STATEMENT

The raw data supporting the conclusions of this article will be made available by the authors without undue reservation.

SUPPORTING INFORMATION

Additional Supporting Information may be found in the online version of this article.

Figure S1. GO and KEGG pathway enrichment analysis for leaves at 10 DAA and for time points: 1.5, 24, and 96 h after exposure to FR.

Figure S2. GO and KEGG pathway enrichment analysis for fruits at 10 DAA and for time points: 1.5, 24, and 96 h after exposure to FR.

Figure S3. Effect of adding far-red (FR) at different plant developmental stages on tomato (*Solanum lycopersicum*), on the total number of fruits at the end of the growth cycle, 74 days after anthesis (DAA).

Figure S4. Representative graph of expression profile across sampling times.

Figure S5. Green group of genes: Temporal expression profiles of differentially expressed genes that were significantly different between FR and No FR at all three time points at leaves.

Figure S6. Orange group of genes: Temporal expression profiles of differentially expressed genes that were significantly different between FR and No FR only at the first time point (1.5 h) at leaves.

Figure S7. Purple group of genes: Temporal expression profiles of differentially expressed genes that were significantly different between FR and No FR only at the last time point (96 h) at leaves.

Figure S8. Temporal expression profiles of differentially expressed genes in fruits.

Data S2. Annotations.

Data S3. AVG_TPMs.

Data S4. Grouping.

Data S5. log2FC.

Data S6. Metabolites (leaves, fruits).

Data S7. Qvalue.

REFERENCES

Ariizumi, T., **Shinozaki, Y.** & **Ezura, H.** (2013) Genes that influence yield in tomato. *Breeding Science*, **63**(1), 3–13.

Ballaré, C.L. & **Pierik, R.** (2017) The shade-avoidance syndrome: multiple signals and ecological consequences. *Plant, Cell & Environment*, **40**(11), 2530–2543.

Binenbaum, J., **Wulff, N.**, **Camut, L.**, **Kiradjiev, K.**, **Anfang, M.**, **Tal, I.** ***et al.*** (2023) Gibberellin and abscisic acid transporters facilitate endodermal suberin formation in Arabidopsis. *Nature Plants*, **9**(5), 785–802.

Borthwick, H.A., **Hendricks, S.B.**, **Parker, M.W.**, **Toole, E.H.** & **Toole, V.K.** (1952) A reversible photoreaction controlling seed germination. *Proceedings of the National Academy of Sciences*, **38**(8), 662–666.

Braun, D.M. (2022) Phloem loading and unloading of sucrose: what a long, strange trip from source to sink. *Annual Review of Plant Biology*, **73**(1), 553–584.

Casal, J.J. (2013) Photoreceptor signaling networks in plant responses to shade. *Annual Review of Plant Biology*, **64**(1), 403–427.

Casal, J.J. & **Fankhauser, C.** (2023) Shade avoidance in the context of climate change. *Plant Physiology*, **191**(3), 1475–1491.

Chen, H., **Bai, S.**, **Kusano, M.**, **Ezura, H.** & **Wang, N.** (2022) Increased ACS enzyme dosage causes initiation of climacteric ethylene production in tomato. *International Journal of Molecular Sciences*, **23**(18), 10788.

Courbier, S., **Grevink, S.**, **Sluijs, E.**, **Bonhomme, P.O.**, **Kajala, K.**, **Van Wees, S.C.** ***et al.*** (2020) Far-red light enhances soluble sugar levels and Botrytis cinerea disease development in tomato leaves in a jasmonate-dependent manner. *BioRxiv*, 2020-05.

De Jong, M., **Wolters-Arts, M.**, **Schimmel, B.C.**, **Stultiens, C.L.**, **de Groot, P.F.**, **Powers, S.J.** ***et al.*** (2015) Solanum lycopersicum AUXIN RESPONSE FACTOR 9 regulates cell division activity during early tomato fruit development. *Journal of Experimental Botany*, **66**(11), 3405–3416.

Demotes-Mainard, S., **Péron, T.**, **Corot, A.**, **Bertheloot, J.**, **Le Gourrierec, J.**, **Pelleschi-Travier, S.** ***et al.*** (2016) Plant responses to red and far-red lights, applications in horticulture. *Environmental and Experimental Botany*, **121**, 4–21.

Fanwoua, J., **de Visser, P.**, **Heuvelink, E.**, **Angenent, G.**, **Yin, X.**, **Marcelis, L.**, & **Struik, P.** (2012) Response of cell division and cell expansion to local fruit heating in tomato fruit. *Journal of the American Society for Horticultural Science*, **137**(5), 294–301.

Forlani, S., **Mizzotti, C.** & **Masiero, S.** (2021) The NAC side of the fruit: tuning of fruit development and maturation. *BMC Plant Biology*, **21**(1), 238.

Franklin, K.A. (2008) Shade avoidance. *New Phytologist*, **179**(4), 930–944.

Gan, L., **Song, M.**, **Wang, X.**, **Yang, N.**, **Li, H.**, **Liu, X.** ***et al.*** (2022) Cytokinins are involved in regulation of tomato pericarp thickness and fruit size. *Horticulture Research*, **9**, uhab041.

García-Hurtado, N., **Carrera, E.**, **Ruiz-Rivero, O.**, **López-Gresa, M.P.**, **Hedden, P.**, **Gong, F.** ***et al.*** (2012) The characterization of transgenic tomato overexpressing gibberellin 20-oxidase reveals induction of parthenocarpic fruit growth, higher yield, and alteration of the gibberellin biosynthetic pathway. *Journal of Experimental Botany*, **63**(16), 5803–5813.

Hu, J., **Israeli, A.**, **Ori, N.** & **Sun, T.P.** (2018) The interaction between DELLA and ARF/IAA mediates crosstalk between gibberellin and auxin signaling to control fruit initiation in tomato. *The Plant Cell*, **30**(8), 1710–1728.

Hu, T., **Ye, J.**, **Tao, P.**, **Li, H.**, **Zhang, J.**, **Zhang, Y.** ***et al.*** (2016) The tomato HD-zip I transcription factor SlHZ 24 modulates ascorbate accumulation through positive regulation of the d-mannose/l-galactose pathway. *The Plant Journal*, **85**(1), 16–29.

Huber, M., **de Boer, H.J.**, **Romanowski, A.**, **van Veen, H.**, **Buti, S.**, **Kahlon, P.S.** ***et al.*** (2024) Far-red light enrichment affects gene expression and architecture as well as growth and photosynthesis in rice. *Plant, Cell & Environment*, **47**(8), 2936–2953.

Huber, M., **Nieuwendijk, N.M.**, **Pantazopoulou, C.K.** & **Pierik, R.** (2021) Light signalling shapes plant–plant interactions in dense canopies. *Plant, Cell & Environment*, **44**(4), 1014–1029.

Hyun, Y. & **Lee, I.** (2006) KIDARI, encoding a non-DNA binding bHLH protein, represses light signal transduction in *Arabidopsis thaliana*. *Plant Molecular Biology*, **61**, 283–296.

Ji, K., **Kai, W.**, **Zhao, B.**, **Sun, Y.**, **Yuan, B.**, **Dai, S.** ***et al.*** (2014) SlNCED1 and SlCYP707A2: key genes involved in ABA metabolism during tomato fruit ripening. *Journal of Experimental Botany*, **65**(18), 5243–5255.

Ji, Y., **Nuñez Ocaña, D.**, **Choe, D.**, **Larsen, D.H.**, **Marcelis, L.F.** & **Heuvelink, E.** (2020) Far-red radiation stimulates dry mass partitioning to fruits by increasing fruit sink strength in tomato. *New Phytologist*, **228**(6), 1914–1925.

Ji, Y., **Ouzounis, T.**, **Schouten, H.J.**, **Visser, R.G.**, **Marcelis, L.F.** & **Heuvelink, E.** (2021) Dissecting the genotypic variation of growth responses to far-red radiation in tomato. *Frontiers in Plant Science*, **11**, 614714.

Jian, W., **Zheng, Y.**, **Yu, T.**, **Cao, H.**, **Chen, Y.**, **Cui, Q.** ***et al.*** (2021) SlNAC6, a NAC transcription factor, is involved in drought stress response and reproductive process in tomato. *Journal of Plant Physiology*, **264**, 153483.

Kalaitzoglou, P., **Van Ieperen, W.**, **Harbinson, J.**, **Van der Meer, M.**, **Martinakos, S.**, **Weerheim, K.** ***et al.*** (2019) Effects of continuous or end-of-day far-red light on tomato plant growth, morphology, light absorption, and fruit production. *Frontiers in Plant Science*, **10**, 322.

Kohnen, M.V., **Schmid-Siegert, E.**, **Trevisan, M.**, **Petrolati, L.A.**, **Sénéchal, F.**, **Müller-Moulé, P.** ***et al.*** (2016) Neighbor detection induces organ-specific transcriptomes, revealing patterns underlying hypocotyl-specific growth. *The Plant Cell*, **28**(12), 2889–2904.

Kou, X., **Zhou, J.**, **Wu, C.E.**, **Yang, S.**, **Liu, Y.**, **Chai, L.** ***et al.*** (2021) The interplay between ABA/ethylene and NAC TFs in tomato fruit ripening: a review. *Plant Molecular Biology*, **106**, 223–238.

Kumar, R., **Khurana, A.** & **Sharma, A.K.** (2013) Role of plant hormones and their interplay in development and ripening of fleshy fruits. *Journal of Experimental Botany*, **65**(16), 4561–4575.

Lacombe, B. & **Achard, P.** (2016) Long-distance transport of phytohormones through the plant vascular system. *Current Opinion in Plant Biology*, **34**, 1–8.

Lee, S., **Lee, S.**, **Yang, K.Y.**, **Kim, Y.M.**, **Park, S.Y.**, **Kim, S.Y.** ***et al.*** (2006) Overexpression of PRE1 and its homologous genes activates gibberellin-dependent responses in *Arabidopsis thaliana*. *Plant and Cell Physiology*, **47**(5), 591–600.

Li, C., **Potuschak, T.**, **Colón-Carmona, A.**, **Gutiérrez, R.A.** & **Doerner, P.** (2005) Arabidopsis TCP20 links regulation of growth and cell division control pathways. *Proceedings of the National Academy of Sciences*, **102** (36), 12978–12983.

Li, H., **Wu, H.**, **Qi, Q.**, **Li, H.**, **Li, Z.**, **Chen, S.** ***et al.*** (2019) Gibberellins play a role in regulating tomato fruit ripening. *Plant and Cell Physiology*, **60**(7), 1619–1629.

Li, L., **Ljung, K.**, **Breton, G.**, **Schmitz, R.J.**, **Pruneda-Paz, J.**, **Cowing-Zitron, C.** ***et al.*** (2012) Linking photoreceptor excitation to changes in plant architecture. *Genes & Development*, **26**(8), 785–790.

Li, L., **van de Kaa, Y.**, **van der Krabben, L.**, **Pierik, R.** & **Kajala, K.** (2025) Effect of low red-to-far-red light on stem elongation and pith cell development in dicots. *Plant Direct*, **9**(4), e70072.

Li, T., **Heuvelink, E.P.** & **Marcelis, L.F.** (2015) Quantifying the source–sink balance and carbohydrate content in three tomato cultivars. *Frontiers in Plant Science*, **6**, 416.

Lu, K.J., **De Rybel, B.**, **Van Mourik, H.** & **Weijers, D.** (2018) Regulation of intercellular TARGET OF MONOPTEROS 7 protein transport in the Arabidopsis root. *Development (Cambridge, England)*, **145**(2), dev152892.

Lucas, W.J., **Groover, A.**, **Lichtenberger, R.**, **Furuta, K.**, **Yadav, S.R.**, **Helariutta, Y.** ***et al.*** (2013) The plant vascular system: evolution, development and functions f. *Journal of Integrative Plant Biology*, **55**(4), 294–388.

Mara, C.D., **Huang, T.** & **Irish, V.F.** (2010) The Arabidopsis floral homeotic proteins APETALA3 and PISTILLATA negatively regulate the BANQUO genes implicated in light signaling. *The Plant Cell*, **22**(3), 690–702.

Martín-Trillo, M. & **Cubas, P.** (2010) TCP genes: a family snapshot ten years later. *Trends in Plant Science*, **15**(1), 31–39.

Matsuo, S., **Kikuchi, K.**, **Fukuda, M.**, **Honda, I.** & **Imanishi, S.** (2012) Roles and regulation of cytokinins in tomato fruit development. *Journal of Experimental Botany*, **63**(15), 5569–5579.

Meijer, D., **Meisenburg, M.**, **van Loon, J.J.** & **Dicke, M.** (2022) Effects of low and high red to far-red light ratio on tomato plant morphology and performance of four arthropod herbivores. *Scientia Horticulturae*, **292**, 110645.

Navaud, O., **Dabos, P.**, **Carnus, E.**, **Tremousaygue, D.** & **Hervé, C.** (2007) TCP transcription factors predate the emergence of land plants. *Journal of Molecular Evolution*, **65**, 23–33.

Ohgishi, M., **Oka, A.**, **Morelli, G.**, **Ruberti, I.** & **Aoyama, T.** (2001) Negative autoregulation of the Arabidopsis homeobox gene ATHB-2. *The Plant Journal*, **25**(4), 389–398.

Okello, R.C., **de Visser, P.H.**, **Heuvelink, E.**, **Lammers, M.**, **de Maagd, R.A.**, **Struik, P.C.** & **Marcelis, L.F.** (2015) A multilevel analysis of fruit growth of two tomato cultivars in response to fruit temperature. *Physiologia plantarum*, **153**(3), 403–418.

Parapunova, V., **Busscher, M.**, **Busscher-Lange, J.**, **Lammers, M.**, **Karlova, R.**, **Bovy, A.G.** ***et al.*** (2014) Identification, cloning and characterization of the tomato TCP transcription factor family. *BMC Plant Biology*, **14**, 1–17.

Park, J., **Lee, Y.**, **Martinoia, E.** & **Geisler, M.** (2017) Plant hormone transporters: what we know and what we would like to know. *BMC Biology*, **15**, 1–15.

Perrot-Rechenmann, C. (2010) Cellular responses to auxin: division versus expansion. *Cold Spring Harbor Perspectives in Biology*, **2**(5), a001446.

Pierik, R. & **Ballaré, C.L.** (2021) Control of plant growth and defense by photoreceptors: from mechanisms to opportunities in agriculture. *Molecular Plant*, **14**(1), 61–76.

Plantenga, F.D., **Bergonzi, S.**, **Bachem, C.W.**, **Visser, R.G.**, **Heuvelink, E.** & **Marcelis, L.F.** (2019) High light accelerates potato flowering independently of the FT-like flowering signal StSP3D. *Environmental and Experimental Botany*, **160**, 35–44.

Renaudin, J.P., **Deluche, C.**, **Cheniclet, C.**, **Chevalier, C.** & **Frangne, N.** (2017) Cell layer-specific patterns of cell division and cell expansion during fruit set and fruit growth in tomato pericarp. *Journal of Experimental Botany*, **68**(7), 1613–1623.

Roig-Villanova, I. & **Martínez-García, J.F.** (2016) Plant responses to vegetation proximity: a whole life avoiding shade. *Frontiers in Plant Science*, **7**, 236.

Sager, J.C., **Smith, W.O.**, **Edwards, J.L.** & **Cyr, K.L.** (1988) Photosynthetic efficiency and phytochrome photoequilibria determination using spectral data. *Transactions of ASAE*, **31**(6), 1882–1889.

Schena, M., **Lloyd, A.M.** & **Davis, R.W.** (1993) The HAT4 gene of Arabidopsis encodes a developmental regulator. *Genes & Development*, **7**(3), 367–379.

Serrani, J.C., **Fos, M.**, **Atarés, A.** & **García-Martínez, J.L.** (2007) Effect of gibberellin and auxin on parthenocarpic fruit growth induction in the cv micro-tom of tomato. *Journal of Plant Growth Regulation*, **26**, 211–221.

Serrani, J.C., **Sanjuán, R.**, **Ruiz-Rivero, O.**, **Fos, M.** & **García-Martínez, J.L.** (2007) Gibberellin regulation of fruit set and growth in tomato. *Plant Physiology*, **145**(1), 246–257.

Shomali, A., **De Diego, N.**, **Zhou, R.**, **Abdelhakim, L.**, **Vrobel, O.**, **Tarkowski, P.** ***et al.*** (2024) The crosstalk of far-red energy and signaling defines the regulation of photosynthesis, growth, and flowering in tomatoes. *Plant Physiology and Biochemistry*, **208**, 108458.

Singh, R., **Rastogi, S.** & **Dwivedi, U.N.** (2010) Phenylpropanoid metabolism in ripening fruits. *Comprehensive Reviews in Food Science and Food Safety*, **9**(4), 398–416.

Song, X., **Gu, X.**, **Chen, S.**, **Qi, Z.**, **Yu, J.**, **Zhou, Y.** ***et al.*** (2024) Far-red light inhibits lateral bud growth mainly through enhancing apical dominance independently of strigolactone synthesis in tomato. *Plant, Cell & Environment*, **47**(2), 429–441.

Steindler, C., **Matteucci, A.**, **Sessa, G.**, **Weimar, T.**, **Ohgishi, M.**, **Aoyama, T.** ***et al.*** (1999) Shade avoidance responses are mediated by the ATHB-2 HD-zip protein, a negative regulator of gene expression. *Development (Cambridge, England)*, **126**(19), 4235–4245.

Su, D., **Liu, K.**, **Yu, Z.**, **Li, Y.**, **Zhang, Y.**, **Zhu, Y.** ***et al.*** (2023) Genome-wide characterization of the tomato GASA family identifies SlGASA1 as a repressor of fruit ripening. *Horticulture Research*, **10**(1), uhac222.

Su, L., **Bassa, C.**, **Audran, C.**, **Mila, I.**, **Cheniclet, C.**, **Chevalier, C.** ***et al.*** (2014) The auxin Sl-IAA17 transcriptional repressor controls fruit size via the regulation of endoreduplication-related cell expansion. *Plant and Cell Physiology*, **55**(11), 1969–1976.

Sun, L., **Sun, Y.**, **Zhang, M.**, **Wang, L.**, **Ren, J.**, **Cui, M.** ***et al.*** (2012) Suppression of 9-cis-epoxycarotenoid dioxygenase, which encodes a key enzyme in abscisic acid biosynthesis, alters fruit texture in transgenic tomato. *Plant Physiology*, **158**(1), 283–298.

Sun, S., **Wang, H.**, **Yu, H.**, **Zhong, C.**, **Zhang, X.**, **Peng, J.** ***et al.*** (2013) GASA14 regulates leaf expansion and abiotic stress resistance by modulating reactive oxygen species accumulation. *Journal of Experimental Botany*, **64**(6), 1637–1647.

Thomas, H., **Van den Broeck, L.**, **Spurney, R.**, **Sozzani, R.** & **Frank, M.** (2022) Gene regulatory networks for compatible versus incompatible grafts identify a role for SlWOX4 during junction formation. *The Plant Cell*, **34** (1), 535–556.

Wang, L. & **Ruan, Y.L.** (2013) Regulation of cell division and expansion by sugar and auxin signaling. *Frontiers in Plant Science*, **4**, 163.

Zažímalová, E., **Murphy, A.S.**, **Yang, H.**, **Hoyerová, K.** & **Hošek, P.** (2010) Auxin transporters—why so many? *Cold Spring Harbor Perspectives in Biology*, **2**(3), a001552.

Zhang, J., **Zhang, Y.**, **Song, S.**, **Su, W.**, **Hao, Y.** & **Liu, H.** (2020) Supplementary red light results in the earlier ripening of tomato fruit depending on ethylene production. *Environmental and Experimental Botany*, **175**, 104044.

Zhen, S. & **Bugbee, B.** (2020) Far-red photons have equivalent efficiency to traditional photosynthetic photons: implications for redefining photosynthetically active radiation. *Plant, Cell & Environment*, **43**(5), 1259–1272.

Zhu, M., **Chen, G.**, **Zhou, S.**, **Tu, Y.**, **Wang, Y.**, **Dong, T.** ***et al.*** (2014) A new tomato NAC (N AM/a TAF1/2/C UC2) transcription factor, SlNAC4, functions as a positive regulator of fruit ripening and carotenoid accumulation. *Plant and Cell Physiology*, **55**(1), 119–135.

Zhu, Z., **Liang, H.**, **Chen, G.**, **Li, F.**, **Wang, Y.**, **Liao, C.** ***et al.*** (2019) The bHLH transcription factor SlPRE2 regulates tomato fruit development and modulates plant response to gibberellin. *Plant Cell Reports*, **38**, 1053–1064.